Petroleum Science 23 (2026) 4753–4772

Contents lists available at ScienceDirect

Petroleum Science

journal homepage: www.keaipublishing.com/en/journals/petroleum-science

Original Paper

Efficient hydrocarbon generation mechanism in low-TOC source rocks of saline lacustrine basins: A case study of the Oligocene Linhe Formation in the Linhe Depression, Hetao Basin

Man Yuan [a,b,c], Jun-Gang Lu [a,b,c,*], Shu-Guang Chen [d], Yu-Lei Shi [d], Ran-Ran Zhou [d], Yi-Ming Fan [a,b,c], Ying-Xuan Lyu [a,b,c], Yi-Nuo Chen [a,b,c], Ming Li [d]

[a] Natural Gas Geology Key Laboratory of Sichuan Province, Chengdu, 610500, Sichuan, China
[b] School of Geoscience and Technology, Southwest Petroleum University, Chengdu, 610500, Sichuan, China
[c] State Key Laboratory of Oil and Gas Reservoir Geology and Exploitation, Southwest Petroleum University, Chengdu, 610500, Sichuan, China
[d] Research Institute of Exploration and Development, Huabei Oilfield Branch of Petro China, Renqiu, 062550, Hebei, China

ARTICLE INFO

Article history:
Received 23 December 2025
Received in revised form
28 January 2026
Accepted 17 May 2026
Available online 21 May 2026

Edited by Min Li

Keywords:
Hydrocarbon generation paradox
Saline lacustrine basin
Low TOC
Linhe Formation
Hetao Basin
Mineral catalysis
Hydrocarbon generation kinetics
Thermochemical sulfate reduction (TSR)

ABSTRACT

The Oligocene Linhe Formation (E_3l) in the Linhe Depression, Hetao Basin, illustrates the "Hydrocarbon Generation Paradox" (the apparent contradiction between low TOC and high hydrocarbon yields). Where lacustrine source rocks with low total organic carbon (TOC, average 1.15%) have produced significant petroleum accumulations, including ultra-deep, high-yield oil flows. To clarify this contradiction, geochemical analyses (TOC, Rock-Eval pyrolysis, GC-MS) and gold-tube pyrolysis experiments were employed to investigate depositional conditions, organic matter characteristics and hydrocarbon generation kinetics of the underlying mechanisms of this paradox. The E_3l source rocks were deposited in hypersaline, strongly reducing lacustrine environment. Low TOC reflects the combined effects of moderate paleoproductivity, effective preservation, and dilution by terrigenous inputs. Hydrocarbon generation kinetics reveal extremely low activation energies (C_{6+} peak at 47 kcal/mol) and high frequency factors, producing an early generation peak ($R_o \approx 0.68\%$). Three enhancement mechanisms: (1) mineral catalysis by illite/smectite clays and pyrite, lowering the reaction barrier; (2) TSR-H_2S feedback, promoting catalytic cracking and yield amplification; and (3) over pressured conditions suppressing secondary cracking while driving episodic expulsion and efficient migration. This study proposes a genetic model of efficient preservation, catalytic hydrocarbon generation, and overpressure-driven expulsion, offering a framework for evaluating low-abundance source rocks in saline lacustrine basins globally.

1. Introduction

Globally, multiple sets of source rocks associated with saline lake and marine saline environments have been extensively developed (Kelts, 1988; Klemme and Ulmishek, 1991). Representative examples include the Lower Cretaceous Lagoa Feia Formation in the Santos Basin, Brazil, the marine shales of the Bakken Formation in the Williston Basin, USA, and the Eagle Ford Formation source rocks in South Texas (Abdi and Rimmer, 2024; Sun et al., 2016; Vivian et al., 2022). In China, salinity-related source rocks are exemplified by the Paleogene Qianjiang Formation and Xingouzui Formation in the Qianjiang Depression of the Jianghan Basin, the Paleogene lower Ganchaigou Formation shales in the Yingxiongling area of the western Qaidam Basin, and the Permian Fengcheng and Lucaogou Formation dolomitic-calcareous shales in the Junggar Basin (Fu et al., 2025; Gong et al., 2024; Li et al., 2021, 2023; Luo et al., 2026; Yang et al., 2025).

Total organic carbon (TOC) content has long been considered a key parameter for assessing source rock quality and hydrocarbon generation capacity (Peters, 1986). Conventional kerogen hydrocarbon generation theory suggests that higher TOC values generally correspond to greater hydrocarbon generation potential (Tissot and Welte, 1984). Nevertheless, exploration, results frequently reveal significant hydrocarbon accumulations in source rocks with moderate or even low TOC (Li et al., 2023; Liu et al.,

* Corresponding author.
E-mail address: lujungang21@swpu.edu.cn (J.-G. Lu).
Peer review under the responsibility of China University of Petroleum (Beijing).

https://doi.org/10.1016/j.petsci.2026.05.024

2024; Zhao et al., 2021). Such observations highlight the importance of additional complex geochemical and geological controls that critically influence hydrocarbon generation within specific depositional settings.

The Linhe Depression of the Hetao Basin in northern China contains two sets of saline lacustrine dark mudstones: the Oligocene Linhe Formation (E_3l) and the Lower Cretaceous Guyang Formation (K_1g) (Fu et al., 2018). Despite an average TOC of approximately 1%, E_3l source rocks have yielded ultra-high oil and gas flows exceeding one thousand tons per day from ultra-deep strata in the northern Xinglong structural belt, creating a "hydrocarbon generation paradox", where high hydrocarbon production occurs despite the low TOC background (Zhang et al., 2023; Wu et al., 2024). Saline lacustrine source rocks typically display low TOC, but exhibit higher hydrocarbon generation efficiency per unit organic matter. Rocks with about 1% TOC can achieve a hydrogen index (HI) comparable to freshwater lacustrine equivalents with 2.0%–2.5% TOC, while their hydrocarbon generation potential can reach 2–2.5 times greater (Gao et al., 2024; Li et al., 2021, 2023; Tang et al., 2021a,b; Yang et al., 2025; Zhi et al., 2021). Some argue that the low TOC may result from the consumption of organic matter during hydrocarbon generation and expulsion (Qin et al., 2007), whereas other studies suggest TOC remains relatively stable throughout the process (Zhong et al., 2004). Li et al. (2023) proposed that saline lacustrine source rocks with low organic abundance exhibit higher hydrocarbon generation and expulsion efficiency. The stratified, saline lacustrine environment favors enrichment of hydrogen-rich, oil-prone organic matter, while associated mineral assemblages may also act as natural catalysts, lowering activation energy for kerogen cracking and substantially increasing generation efficiency thereby greatly enhancing hydrocarbon generation efficiency beyond what would be predicted based on TOC content alone (Fu et al., 2024; Lewan, 1998; Rahman et al., 2018; Wang et al., 2023). Although previous studies have confirmed the basic geological characteristics and petroleum potential of the Linhe Depression, significant deficiencies remain in the understanding of its hydrocarbon generation process, efficiency, and controlling factors (Fu et al., 2018; Wu et al., 2024; Zhang et al., 2023).

To address the hydrocarbon generation paradox of low TOC yet high resource potential, a multi-method integrated research strategy was used. Core samples from the Oligocene E_3l in the Linhe Depression of the Hetao Basin were systematically collected and analyzed using TOC measurement, Rock-Eval pyrolysis, X-ray diffraction (XRD), saturated hydrocarbon gas chromatography-mass spectrometry (GC-MS), and gold-tube pyrolysis experiments. These approaches facilitated source rock evaluation, sedimentary environment analysis, and to investigate the main controlling factors behind the development of low-TOC source rocks and the genetic mechanisms responsible for their high resource potential. The findings provide a theoretical basis and a case study reference for the evaluation of source rock basins characterized by low TOC and high resource potential worldwide.

2. Regional geology

The Hetao Basin in northern China is a Mesozoic–Cenozoic rift-superimposed sedimentary basin (Fig. 1(a)) (Zhang et al., 2023). Its structural framework is governed by the North China Craton, the Alxa Block, and the Central Asian Orogenic Belt (Dong et al., 2019). The basin is bounded to the south by the northern marginal fault of the Ordos Basin, and to the north by the piedmont fault zones of the Lang, Seerteng, and Daqing mountains, adjacent to the Yinshan Structural Zone. Since the Late Mesozoic to Cenozoic, the counterclockwise rotation of the Ordos Block, driven by the eastward extrusion of crustal fragments from the northeastern Tibetan Plateau has controlled crustal extension in the Hetao Basin and associated orogenic activity (Zhang, 2019). Sedimentary thickness-fault system relationships divide the Hetao Basin into five first-order tectonic units, from west to east: Linhe Depression, Wulashan Uplift, Wuqian Depression, Baotou Uplift, and Hohhot Depression (Li et al., 2022). The Linhe Depression, the principal oil-generating unit, trends NE-SW, covers approximately 2.24 × 10^3 km^2, and exhibits a structural framework subdivided into northern and southern zones, further segmented into eastern and western belts (Fig. 1(b)) (Fu et al., 2018; Zhang et al., 2023). The study area lies in the north-central part of the central bulge area of the Linhe Depression (Fig. 1(c)).

Stratigraphy of the Linhe Depression comprises, in ascending order, the Cretaceous, Paleogene, Neogene, and Quaternary systems (Fig. 1(d)). Previous studies have shown that two sets of lacustrine dark mudstones—the Lower Cretaceous Guyang Formation (K_1g) and the Oligocene Linhe Formation (E_3l)—represent the primary source rock intervals (Fig. 1(d)) (Fu et al., 2018; Lu et al., 2022).

3. Samples and methods

3.1. Samples

For this study, source rock sampling was conducted in 5 wells (HT1, XH1, XH5, XH12-2, and LH1X) located in the Xinglong Structural Belt of the Linhe Depression, Hetao Basin. A total of 105 samples were collected, with their locations shown in Fig. 1(c). The samples were obtained from the following wells: HT1 ($N = 20$), XH1 ($N = 30$), XH5 ($N = 15$), XH12-2 ($N = 20$), and LH1X ($N = 20$). The samples underwent XRD, TOC analysis, Rock-Eval pyrolysis, GC-MS, and gold-tube pyrolysis experiments. The XRD, TOC, Rock-Eval pyrolysis, and GC-MS were performed at the Experimental Center of Huabei Oilfield Company, PetroChina Co. Ltd., while the gold-tube pyrolysis experiments were conducted at the Guangzhou Institute of Geochemistry, Chinese Academy of Sciences.

3.2. Methods

3.2.1. X-ray diffraction (XRD)

XRD analysis was performed on 15 samples collected from wells XH5, LH1X, and XH12-2 using an X-ray diffractometer. Different types of mineral crystals exhibit specific X-ray diffraction patterns. The mineral content in a sample is positively correlated with the intensity of the characteristic peaks. This correlation, expressed as the K-value, enables quantitative determination of mineral content. Non-clay mineral content in sedimentary rocks is typically determined using the K-value method, while total clay mineral content is determined either by the K-value method or water suspension separation. Experiments were conducted under ambient temperatures of 15–25 °C and relative humidity ≤70%. Experimental conditions included Cu-Kα radiation; a divergence slit and scattering slit both set at 1°; a receiving slit of 0.3 mm. Operating voltage and current were 40 kV and 40 mA, respectively. Continuous scanning was applied over 5°–45° at 2°/min with a sampling interval of 0.02. Sedimentary rock samples were crushed and ground to powder. Clay minerals <2 μm were extracted via suspension or centrifugation. Natural, ethylene glycol-saturated XRD, and high-temperature XRD analyses were employed to identify clay mineral types based on diffraction peak variations. The remaining sample powder was weighed, and clay minerals <10 μm were separated. From this fraction, the total clay content was determined by either the weighing method or the K-value method. The content of each non-clay mineral was then measured

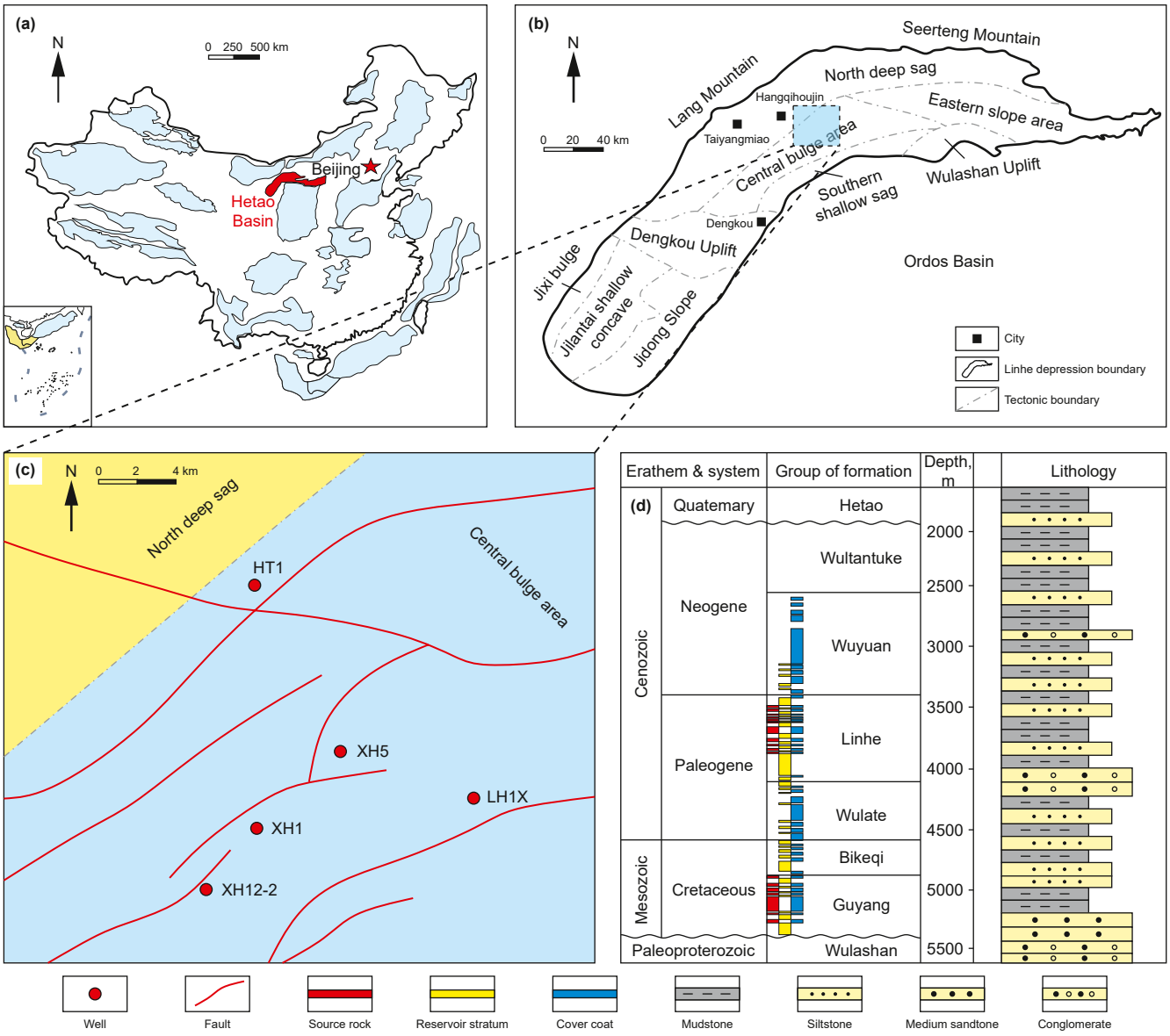

Fig. 1. Structural location map and stratigraphic column of the Linhe Depression, Hetao Basin (Fu et al., 2018; Li et al., 2022; Lu et al., 2022; Zhang et al., 2023). (**a**) Geographic location of the Hetao Basin in China; (**b**) Structural location of the Linhe Depression, Hetao Basin; (**c**) Locations of sampling wells in the study area; (**d**) Comprehensive stratigraphic column of the Hetao Basin.

using the K-value method, and relative mineral proportions were calculated by normalizing the sum of non-clay and clay mineral contents to 100% (Wu et al., 2024).

3.2.2. TOC analysis and Rock-Eval pyrolysis

TOC measurement and Rock-Eval pyrolysis were performed on all samples obtained from wells HT1, XH1, XH5, XH12-2, and LH1X. TOC content was determined using a LECO elemental analyzer. Rock-Eval pyrolysis of these samples was conducted using a Rock-Eval II instrument (Peters, 1986). The specific experimental procedure was as follows: the sample was first heated to 300 °C and held constant for 3 min, then heated to 600 °C at a rate of 25 °C/min. The amounts of free hydrocarbons in volatile components (S_1) and the amounts of hydrocarbons generated from the cracking of heavy hydrocarbons (S_2) were determined separately. S_3 represents the amount of CO_2 produced during the pyrolysis process. T_{max}, the temperature corresponding to the S_2 peak, denotes the pyrolysis peak temperature (Xiao et al., 2021).

3.2.3. Saturated hydrocarbon gas chromatography-mass spectrometry (GC-MS)

A total of 38 samples from wells HT1, XH1, XH5, XH12-2, and LH1X were selected for GC-MS experiments. Samples were cleaned, crushed, and pulverized prior to testing. Following the SY 5258-1991 (1991) (Chinese petroleum and natural gas industry standard), saturated hydrocarbon fractions were analyzed using a HP5890-5972 gas chromatograph/mass spectrometer. In accordance with SY/T 5779-1995 (1995), total hydrocarbon gas chromatography of the source rock extracts was determined using an HP5890 II gas chromatograph. Soxhlet extraction was performed with a chloroform/methanol (87:13) solvent mixture for 72 h. Extractable organic matter was separated by column chromatography into saturated hydrocarbons, aromatic hydrocarbons, and non-hydrocarbons.

Saturated hydrocarbon fractions were analyzed using a Thermo MS-6068 gas chromatography-mass spectrometry (GC-MS) system equipped with a DB-1MS flexible quartz capillary column

Table 1
Basic information of samples for gold-tube pyrolysis experiments.

Well	Depth, m	TOC, %	T_{max}, °C	S_1+S_2, mg HC/g rock	HI, mg HC/g TOC	R_o, %
XH12-2	5241.19	1.05	406	2.95	197.14	0.57

(60 m × 0.320 mm × 0.25 μm). Helium served as the carrier gas in a constant flow mode of 1.2 mL/min. The GC oven program consisted of an initial temperature of 100 °C for 4 min; increased to 210 °C at 2.5 °C/min; then raised to 305 °C at 1.7 °C/min and held for 15 min. Scanning modes included total ion current (TIC) and selected ion monitoring (SIM). The ion source temperature was set at 250 °C, and the electron energy was 70 eV. Compounds were identified based on characteristic ions and chromatographic retention times.

3.2.4. Gold-tube pyrolysis experiments

Low-maturity hydrocarbon source rock samples (R_o = 0.57%) from Well XH12-2 were selected for gold-tube pyrolysis experiments (Table 1). Selection was based on the following criteria: (1) organic matter type is Type II, consistent with the dominant type in E_3l source rocks of the study area; (2) immature to low-maturity state, ensures kerogen retains full hydrocarbon generation potential, suitable for thermal simulations; (3) TOC and HI values are representative of regional samples; (4) mineral assemblage includes major types commonly present in source rocks, with catalytic components such as I/S, pyrite, anhydrite, and carbonate. This assemblage enables effective simulation of synergistic catalytic effects under geological conditions. Pressure was maintained at 50 MPa with pressure fluctuations below 1 MPa. The heating program involved rapid ramping from ambient temperature to 250 °C (held for 8 h), followed by two groups ascending to 600 °C at rates of 20 and 2 °C/h, respectively. The target temperature range was 300–600 °C, encompassing 24 experimental temperature points. Detailed procedures for the gold-tube pyrolysis experiments can be referenced from previous studies (Liang et al., 2020a, 2020b). After pyrolysis, products were subjected to qualitative and quantitative analysis. The pyrolysis products in this study comprised hydrocarbon gases, non-hydrocarbon gases, and liquid hydrocarbons.

3.2.5. Calculation of kinetic parameters

The experimental data obtained from the gold-tube pyrolysis experiments were processed using the KINETIC 2000 software for kinetic parameters. The calculation of kinetic parameters was based on methodologies established in previous studies (Burnham et al., 1987; Schenk and Dieckmann, 2004).

4. Results

4.1. Mineral composition characteristics

The E_3l source rocks exhibit generally homogeneous mineral composition, dominated by clay minerals and quartz, with frequent carbonate minerals and minor feldspar, pyrite, anhydrite, and analcime in some samples (Fig. 2). Clay content ranges from 13.00% to 67.00% (average 47.62%), while quartz ranges from 2.00% to 40.00% (average 21.57%). Feldspar consists mainly of K-feldspar and plagioclase, with contents ranging from 0.20% to 2.00% (average 1.19%), and from 2.00% to 9.00% (average 5.93%), respectively. Pyrite, anhydrite, and analcime occur in lower abundances, with contents ranging from 2.00% to 10.00% (average 4.39%), 0.90%-12.60% (average 4.78%), and from 2.00% to 7.00% (average 3.41%), respectively. Carbonate mineral composition varies among wells. In XH5, calcite dominates (3.00%–18.00%, average 10.88%), with negligible dolomite (0%–0.30%, average 0.30%). In contrast, LH1X and XH12-2 are dolomite rich, (1.00%–73.00%, average 28.68%), with calcite ranging from 0% to 41.00% (average 8.20%) (Table 2; Fig. 2(a)).

Clay minerals are primarily illite/smectite mixed-layer (I/S), ranging from 51.00% to 86.00% (average 74.27%). Illite and chlorite occur in lower proportions ranging from 9.00% to 6.00% (average 18.60%) and 2.00%–3.00% (average 7.13%), respectively (Table 2; Fig. 2(b)).

4.2. Total organic carbon (TOC) and Rock-Eval

TOC and Rock-Eval pyrolysis analyses were performed on 105 mudstone samples from 5 wells in the study area. TOC values range from 0.03 to 3.97 wt% (average 1.15 wt%), hydrocarbon

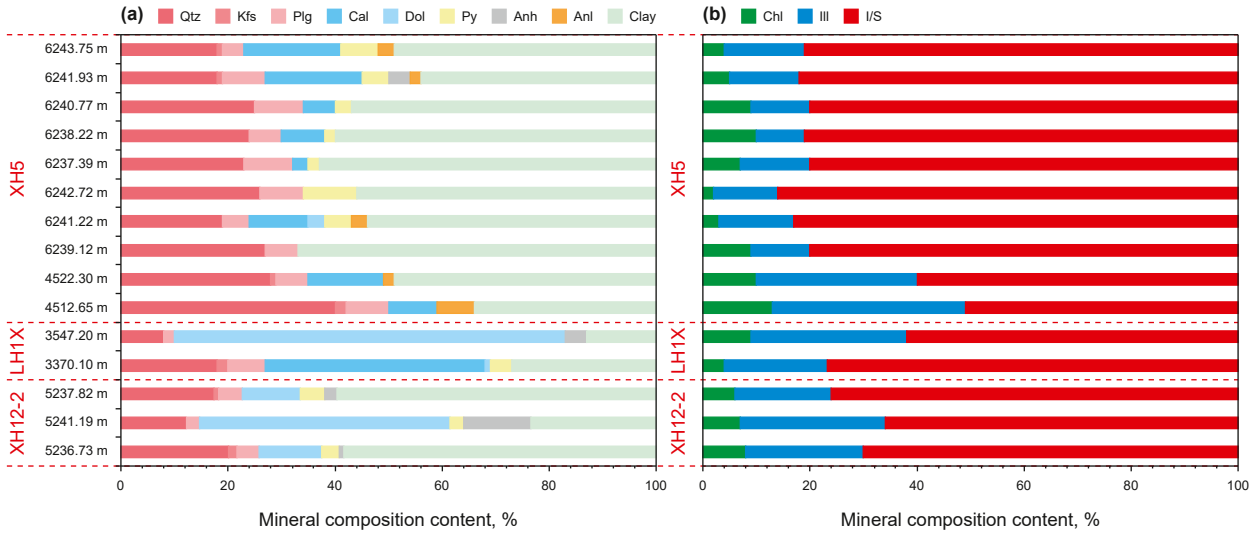

Fig. 2. Mineral composition of the E_3l source rock samples from the Linhe Depression, Hetao Basin. (**a**) Bulk mineral composition; (**b**) Clay mineral composition.

Table 2
Mineral composition of the E_3l source rock, Linhe Depression, Hetao Basin.

Well	Depth, m	Lithology	Qtz, %	Kfs, %	Plg, %	Cal, %	Dol, %	Py, %	Anh, %	Anl, %	Clay, %	Chl, %	Ill, %	I/S, %
XH5	5236.70	Mudstone	40	2	8	9	/	/	/	7	34	13	36	51
XH5	5241.19	Mudstone	28	1	6	14	/	/	/	2	49	10	30	60
XH5	5237.92	Mudstone	27	/	6	/	/	/	/	/	67	9	11	80
XH5	3371.00	Mudstone	19	/	5	11	3	5	/	3	54	3	14	83
XH5	3550.00	Mudstone	26	/	8	/	/	10	/	/	56	2	12	86
XH5	4512.40	Mudstone	23	/	9	3	/	2	/	/	63	7	13	80
XH5	4521.30	Mudstone	24	/	6	8	/	2	/	/	60	10	9	81
XH5	6239.12	Mudstone	25	/	9	6	/	3	/	/	57	9	11	80
XH5	6241.22	Mudstone	18	1	8	18	/	5	4	2	44	5	13	82
XH5	6242.72	Mudstone	18	1	4	18	/	7		3	49	4	15	81
XH12-2	5236.70	Mudstone	20.1	1.5	4.2	/	11.7	3.3	0.9	/	58.3	8	22	70
XH12-2	5241.19	Mudstone	12.1	0.2	2.4	/	46.8	2.5	12.6	/	23.4	7	27	66
XH12-2	5237.92	Mudstone	17.4	0.8	4.4	/	10.9	4.5	2.4	/	59.6	6	18	76
LH1X	3371.00	Mudstone	18	2	7	41	1	4	/	/	27	5	19	76
LH1X	3550.00	Mudstone	8	/	2	/	73	/	4	/	13	9	29	62

Table 3
TOC and rock-eval pyrolysis data of E_3l source rocks, Linhe Depression, Hetao Basin.

Well	TOC, wt%	S_1+S_2, mg HC/g rock	T_{max}, °C	HI, mg HC/g TOC	PI
HT1 ($N = 20$)	0.08–1.76	0.11–6.74	400–445	65.17–317.89	0.09–0.46
	0.76	2.64	422.15	212.82	0.26
XH1 ($N = 30$)	0.03–1.56	0.13–6.81	418–439	63.90–670.47	0.04–0.34
	0.51	1.83	426.07	327.49	0.17
XH5 ($N = 15$)	0.83–3.02	2.07–14.59	382–435	236.76–772.97	0.03–0.58
	1.70	8.01	426.47	386.56	0.16
XH12-2 ($N = 20$)	0.11–3.97	1.11–20.69	417–441	209.09–844.14	0.01–0.33
	1.84	9.74	433.95	486.38	0.08
LH1X ($N = 20$)	0.54–2.97	1.35–15.38	416–447	230.91–533.70	0.02–0.27
	1.37	5.74	429.90	353.76	0.07
All sample ($N = 105$)	0.03–3.97	0.11–20.69	382–447	63.90–844.14	0.01–0.58
	1.15	5.12	427.61	349.36	0.15

Note: 1. "N" is the number of source rock samples; 2. HI: hydrogen index = S_2/TOC×100; 3. PI: production index = $S_1/(S_1+S_2)$.

generation potential (S_1+S_2) range from 0.11 to 20.69 mg HC/g rock), T_{max} range from 3.82 to 447 °C (average 427.61 °C), hydrogen index (HI) range from 63.90 to 844.14 mg HC/g TOC (average 349.36 mg HC/g TOC), and from 0.01 to 0.58 (average 0.15) (Table 3). Among them, samples from wells XH5 and XH12-2 exhibit significantly higher TOC, S_1+S_2, and HI values compared to those from wells LH1X, HT1, and XH1.

4.3. Biomarker characteristics of source rock

4.3.1. n-Alkanes and isoprene alkanes

GC-MS analysis was performed on 38 mudstone samples from 5 wells in the study area. The results indicate that the samples are dominated by short-chain *n*-alkanes and cycloalkanes, with the highest abundance observed in the nC_{15}–nC_{22} range. The carbon preference index (CPI) ranges from 0.91 to 1.43 (average 1.10). Pristane (Pr) and phytane (Ph) were detected in all samples, with Pr/Ph ratios ranging from 0.2 to 1.76 (average 0.62). The Pr/nC_{17} and Ph/nC_{18} ratio ranges from 0.21 to 3.93 (average 0.58), from 0.27 to 4.63 (average 1.54), respectively (Table 4; Fig. 3(a) and (b)).

4.3.2. Carotane

Among the 38 mudstone samples, 16 samples from wells HT1, XH1, and LH1X showed relatively high abundances of γ-carotane and β-carotane. The relative abundance relationship between the two is consistently characterized by a higher abundance of γ-carotane than β-carotane (Fig. 3(a) and (b)). The γ-carotane index and β-carotane index range from 0.004 to 0.112 (average 0.034) and from 0.003 to 0.071 (average 0.026), respectively (Table 4).

4.3.3. Pentacyclic triterpene

The hopane distributions in the source rocks are relatively consistent, predominantly characterized by high abundances of C_{30} hopane along with elevated levels of gammacerane. Some samples exhibit an "upward tailing" distribution of C_{31}–C_{35} homohopanes (Fig. 3(c) and (d)). The Gammacerane/C_{30} hopane (Gam/C_{30}H) ratio ranges from 0.11 to 1.86 (average 0.68) (Table 4).

4.3.4. Steranes

The distribution of C_{27}, C_{28}, and C_{29} steranes in the E_3l source rocks from the study area exhibits an inverted "L"-shaped pattern (Fig. 3(e) and (f)). The relative contents of the three components range from 13.47% to 28.50% (average 21.90%), from 14.07% to 29.57% (average 23.15%), and from 46.64% to 64.33% (average 54.95%), respectively. The $C_{29}\beta\beta/(\alpha\alpha+\beta\beta)$ ratio ranges from 0.20 to 0.50 (average 0.28), and the C_{29}20S/(20S + 20R) ratio ranges from 0.10 to 0.45 (average 0.26) (Table 4).

4.4. Results of gold-tube pyrolysis experiments

4.4.1. Characteristics of hydrocarbon generation products

Gold-tube pyrolysis experiments at heating rates of 20 °C/h and 2 °C/h produced hydrocarbon and non-hydrocarbon components (C_1, C_2, C_3, $C_{4\text{-}5}$, $C_{6\text{-}14}$, C_{14+}, and H_2S) (Table 5). Hydrocarbon yield trends with temperature were consistent under both heating rates (Fig. 4). At 2 °C/h, prolonged reaction time facilitated more complete kerogen decomposition, resulting in higher organic matter conversion rates and hydrocarbon yields. This heating rate is more suitable for characterizing the complete hydrocarbon generation process. However, since the yield of the C_{14+} fraction peaked immediately at the initial temperature under 2 °C/h, subsequent analyses were based on 20 °C/h data to avoid statistical bias.

At 20 °C/h, gaseous hydrocarbons exhibited an initial increase followed by decline with rising temperature (Fig. 4(a)–(d)). Under heating rate of, the peak hydrocarbon yields of C_1, C_2, C_3, and $C_{4\text{-}5}$ are 50.45 mg/g TOC (EasyR_o = 3.32%), 12.93 mg/g TOC (EasyR_o = 2.19%), 9.83 mg/g TOC (EasyR_o = 1.81%), and 7.31 mg/g TOC (EasyR_o = 1.81%), respectively (Table 5). Among the non-hydrocarbon gases, H_2S exhibits the highest yield, showing an initial increase followed by a decrease with rising temperature, with a peak yield of 222.28 mg/g TOC (EasyR_o = 3.32%) (Table 5).

Table 4
Main biomarker parameters of E_3l source rocks, Linhe Depression, Hetao Basin.

Well	Depth, m	Lithology	TIC						*m/z* 191	*m/z* 217				
			1	2	3	4	5	6	7	8	9	10	11	12
HT1	5885.00	Mudstone	1.21	0.42	0.47	/	/	1.16	0.14	24.81	24.12	51.07	0.32	0.35
HT1	5978.00	Mudstone	0.58	0.36	0.57	/	/	1	0.34	19.48	24.82	55.71	0.34	0.42
HT1	6017.67	Mudstone	1.66	0.67	0.48	/	/	1.43	0.16	19.32	25.26	55.42	0.36	0.41
HT1	6019.44	Mudstone	1.24	0.33	0.32	0.004	0.004	1.14	0.25	13.47	22.97	63.56	0.41	0.44
HT1	6020.61	Mudstone	1.66	0.57	0.41	/	/	1.11	0.20	23.56	29.17	47.27	0.36	0.42
HT1	6022.07	Mudstone	0.8	0.21	0.27	/	/	1.12	0.21	23.72	26.38	49.90	0.34	0.42
HT1	6023.01	Mudstone	1.53	3.93	1.77	/	/	0.91	0.13	26.22	24.85	48.93	0.36	0.39
HT1	6025.21	Mudstone	1.76	0.55	0.31	0.007	0.003	1.12	0.11	17.85	23.01	59.14	0.32	0.40
HT1	6131.00	Mudstone	0.52	0.48	1.18	0.046	0.038	0.97	0.96	18.51	21.10	60.40	0.47	0.44
HT1	6156.00	Mudstone	0.57	0.49	1.39	0.038	0.041	1.01	0.71	18.94	23.99	57.08	0.44	0.44
HT1	6197.00	Mudstone	0.67	0.39	0.86	/	/	0.99	0.35	21.58	25.23	53.19	0.32	0.42
HT1	6270.00	Mudstone	0.51	0.58	1.12	/	/	1	1.00	20.63	21.53	57.84	0.50	0.45
HT1	6324.00	Mudstone	0.5	0.49	1.14	/	/	0.98	0.45	18.75	22.39	58.86	0.48	0.44
XH1	4197.00	Mudstone	0.31	0.32	1.96	0.034	0.025	1.2	0.57	24.93	23.88	51.20	0.24	0.18
XH1	4215.00	Mudstone	0.21	0.27	3.5	0.112	0.071	1	0.54	21.07	26.35	52.58	0.23	0.10
XH1	4235.32	Mudstone	0.66	0.39	1.68	/	/	1.22	0.29	28.50	24.86	46.64	0.29	0.29
XH1	4238.41	Mudstone	0.87	0.66	1.43	0.006	0.005	1.24	0.60	22.80	29.57	47.64	0.22	0.12
XH1	4238.44	Mudstone	0.52	0.32	0.52	0.007	0.005	1.21	0.28	23.50	28.28	48.21	0.24	0.11
XH1	4238.88	Mudstone	0.42	0.42	1.42	/	/	1.27	0.16	21.63	25.30	53.07	0.23	0.15
XH1	4242.96	Mudstone	0.26	0.35	0.89	0.065	0.051	1	1.07	23.36	21.87	54.77	0.27	0.28
XH1	4243.12	Mudstone	0.46	0.28	0.56	/	/	1.05	0.55	22.93	22.43	54.65	0.25	0.27
XH1	4324.00	Mudstone	0.45	0.35	0.81	0.012	0.008	1.01	0.23	24.33	22.78	52.89	0.24	0.25
XH1	4378.00	Mudstone	0.37	0.5	1.42	0.040	0.037	1.03	0.91	21.82	24.15	54.04	0.23	0.14
XH1	4468.00	Mudstone	0.38	0.66	1.81	0.006	0.005	1.01	0.94	22.55	19.54	57.91	0.23	0.14
XH1	4531.00	Mudstone	0.38	0.54	1.51	0.051	0.039	1	1.86	27.43	19.13	53.44	0.24	0.19
XH1	4596.00	Mudstone	0.48	0.73	1.60	0.029	0.020	1.01	1.51	27.13	19.61	53.26	0.22	0.19
XH1	4668.00	Mudstone	0.47	0.66	1.40	0.069	0.059	0.98	1.08	24.99	21.65	53.36	0.22	0.17
XH5	4450.00	Mudstone	0.64	0.42	0.94	/	/	1.18	0.30	22.70	22.33	54.98	0.24	0.18
XH5	4578.00	Mudstone	0.5	0.5	1.28	/	/	1.14	0.33	22.86	22.65	54.49	0.26	0.22
XH5	4650.00	Mudstone	0.42	0.75	2.04	/	/	0.99	0.57	21.60	14.07	64.33	0.20	0.13
XH5	4748.00	Mudstone	0.34	0.39	1.11	/	/	0.99	1.23	24.06	21.31	54.63	0.21	0.21
XH5	4804.00	Mudstone	0.59	0.84	1.48	/	/	0.99	0.73	19.99	18.72	61.29	0.21	0.18
XH12-2	4993.00	Mudstone	0.4	1.04	2.41	/	/	1	0.77	17.08	22.79	60.13	0.23	0.20
LH1X	3338.00	Mudstone	0.23	0.31	3.79	0.015	0.011	1.39	1.22	17.87	22.12	60.00	0.22	0.12
LH1X	3462.00	Mudstone	0.34	0.48	1.5	/	/	1	1.82	22.00	22.98	55.02	0.20	0.10
LH1X	3444.00	Mudstone	0.23	0.69	4.63	/	/	1.36	1.01	19.83	21.15	59.02	0.22	0.11
LH1X	3572.00	Mudstone	0.2	0.41	4.29	/	/	1.37	1.10	20.71	22.97	56.32	0.24	0.10
LH1X	3709.00	Mudstone	0.23	0.43	4.18	/	/	1.33	0.99	19.54	24.58	55.88	0.23	0.10

Note:1. Pr/Ph = Pristane/Phytane; 2. Pr/nC_{17} = Pristane/nC_{17}; 3. Ph/nC_{18} = Pytane/nC_{18}; 4. γ-carotane index = γ-carotane/predominant carbon number; 5. β-carotane index = β-carotane/prodomonant carbon number; 6. CPI; 7. Gam/C_{30}H = Gammacerane/C_{30} hopane; 8. C_{27} regular steranes = $C_{27}/(C_{27}+C_{28}+C_{29})$ regular steranes (%); 9. C_{28} regular steranes = $C_{28}/(C_{27}+C_{28}+C_{29})$ regular steranes (%); 10. C_{29} regular steranes = $C_{29}/(C_{27}+C_{28}+C_{29})$ regular steranes (%); 11. $C_{29}\beta\beta/(\alpha\alpha+\beta\beta)$; 12. C_{29}20S/(20S + 20R).

Liquid hydrocarbons reach their peak yields at relatively low temperatures, with maximum yields of $C_{6\text{-}14}$ and C_{14+} being 12.44 mg/g TOC (EasyR_o = 1.19%) and 133.35 mg/g TOC (EasyR_o = 0.68%), respectively (Table 5; Fig. 4(e) and (f)).

The early peak in liquid hydrocarbon generation likely reflects preferential formation of high-molecular-weight hydrocarbons in a closed system, followed by progressive cracking into lower-molecular-weight hydrocarbons at elevated temperatures. As temperature further increases, hydrocarbon yields gradually decline after reaching their maxima, primarily due to the cracking rate exceeding the generation rate or reactions between hydrocarbons and minerals. Additionally, high-molecular-weight hydrocarbons ultimately crack into methane (Tissot and Welte, 1984; Tang et al., 2009; Wang et al., 2013; Zhang et al., 2026).

4.4.2. Kinetic characteristics of hydrocarbon generation

During geological evolution, the hydrocarbon generation in source rocks involves continuous physicochemical reactions controlled by time, temperature, and pressure (Tissot and Welte, 1984). Activation of different chemical bonds at successive maturity stages produces distinct product compositions (Behar et al., 1997). Kerogen transformation follows a multi-parallel first-order reaction kinetic model (Behar et al., 1997; Peters et al., 2015). To quantify hydrocarbon generation behavior, thermal simulation data were processed using KINETICS software yielding kinetic parameters for C_1, $C_{2\text{-}5}$, $C_{1\text{-}5}$, $C_{6\text{-}14}$, and C_{6+} (Figs. 5 and 6).

The measured values of gaseous and liquid hydrocarbons generated during the thermal simulation show good agreement with the fitted trends, demonstrating the validity of the kinetic parameters (Figs. 5 and 6). The activation energy of C_1 ranged from 43 to 66 kcal/mol, with a peak at 60 kcal/mol (accounting for 40.13%), and a frequency factor of 8.80×10^{11} S^{-1} (Fig. 5(a)). The activation energy of $C_{2\text{-}5}$ ranged from 42 to 56 kcal/mol, with a peak at 52 kcal/mol (25.54%), and a frequency factor of 2.91×10^{11} S^{-1} (Fig. 5(c)). The activation energy of $C_{1\text{-}5}$ ranged from 41 to 62 kcal/mol, exhibiting a bimodal distribution with two obvious peaks of 53 kcal/mol (18.78%) and 58 kcal/mol (18.42%), and a frequency factor of 1.95×10^{11} S^{-1} (Fig. 5(e)). The activation energy of $C_{6\text{-}14}$ ranged from 41 to 56 kcal/mol, with a peak at 49 kcal/mol, and a frequency factor of 1.24×10^{13} S^{-1} (Fig. 6(a)). The activation energy of C_{6+} ranged from 42 to 52 kcal/mol, with a peak at 47 kcal/mol, and a frequency factor of 2.60×10^{13} S^{-1} (Fig. 6(c)).

5. Discussions

5.1. Hydrocarbon generation potential of source rock

TOC and S_1+S_2 are key indicators of source rocks' hydrocarbon generation potential (Peters, 1986). A steeper slope between S_1+S_2

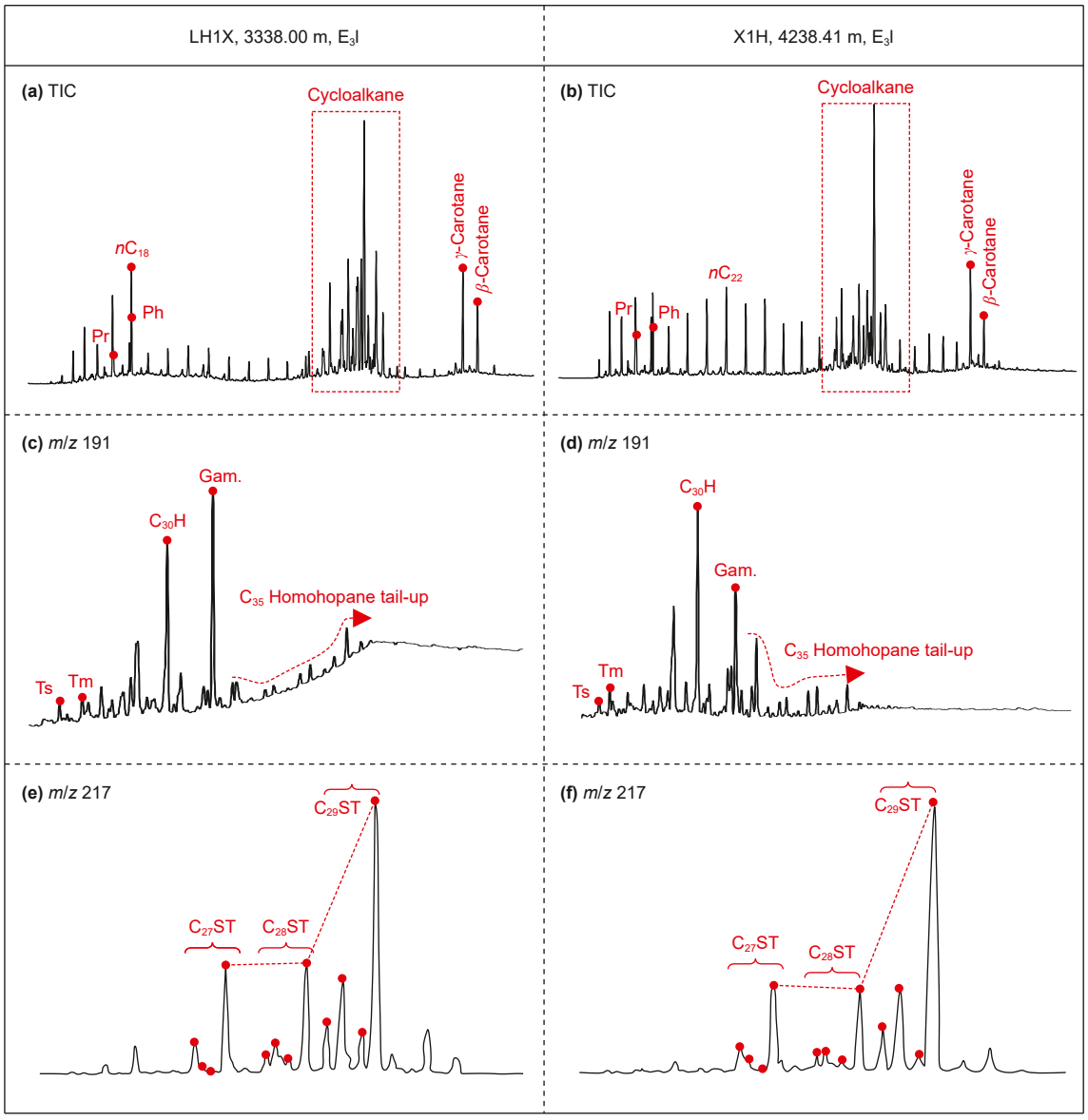

Fig. 3. Gas chromatograms and mass spectrograms of mudstone of the E_3l source rock, Linhe Depression, Hetao Basin. Note: Pr = Pristane; Ph = Phytane; Ts = 18α(H), 21β(H)-22,29,30-trisnorneohopane; Tm = 17α(H), 21β(H)-22,29,30-trisnorneohopane; H = Hopane; Gam. = Gammacerane; ST = Sterane.

and TOC generally reflects stronger generation capacity. Correlation analysis based on saline lacustrine basin criteria shows that most samples fall within fair to excellent categories (Fig. 7(a)). However, well XH1 exhibits a markedly lower slope, consistent with its lowest TOC (average 0.51 wt%) and S_1+S_2 (average 1.83 mg/g) among these wells, indicating a relatively poor hydrocarbon generation potential. Meanwhile, its lower HI reveals a relatively low proportion of hydrogen-rich active components in its organic matter. The relatively higher PI (average 0.17) and T_{max} values in XH1 suggest that its thermal maturity may be slightly higher than that of the other wells, as part of the active components have been preferentially converted during geological history.

T_{max} and HI provide insight into organic matter type, with only minor inter-well variations (Fig. 7(b)). Similar results were obtained using the PI-T_{max} (Fig. 7(c)). The Ph/nC$_{18}$-Pr/nC$_{17}$ proposed by Tribovillard et al. (2009) can be used to determine organic matter type and maturity. The organic matter in the samples is predominantly derived from aquatic sources, with well HT1 showing a relatively higher input of terrestrial organic matter (Fig. 8(b)). All results indicate that the organic matter types of the E_3l source rocks are distributed across Types I-III, with Type II_1 and Type II_2 being predominant. The samples from the study area are characterized by early hydrocarbon generation and expulsion, resulting in an earlier S_2 peak and consequently lower measured T_{max} values (Fu et al., 2025; Wu et al., 2024; Zhang et al., 2007). Although T_{max} suggests immature to early-mature stages, sterane isomerization (Peters et al., 2005; Tribovillard et al., 2009) indicate that HT1 samples are predominantly mature, whereas other wells remain low maturity (Fig. 8). This highlights the tendency of T_{max} to underestimate maturity in early-generation source rocks.

5.2. Depositional environment of source rock

Pr/Ph is commonly used to determine the depositional environment of source rocks (Peters et al., 2005). Except for some samples from HT1 that fall within the redox transition zone, most samples indicate strongly reducing conditions (Fig. 9(a)). Redox conditions inferred from Fig. 8(b) are consistent with these results

Table 5
Hydrocarbon and H_2S yields from gold-tube pyrolysis experiments of E_3l source rocks.

Heating rate, °C/h	*T*, °C	EasyR_o, %	Gaseous hydrocarbon yields, mg/g TOC				Liquid hydrocarbon yields, mg/g TOC		H_2S, mg/g TOC
			C_1	C_2	C_3	C_{4-5}	C_{6-14}	C_{14+}	
20	336.2	0.57	0.49	0.08	0.07	0.04	2.07	103.44	1.21
	360.0	0.68	1.42	0.50	0.62	0.52	3.75	133.35	11.40
	384.0	0.80	1.93	1.13	1.16	0.81	7.40	125.10	12.75
	408.0	0.96	3.57	2.60	2.45	1.71	9.91	101.27	20.56
	432.0	1.19	6.37	4.93	4.46	3.13	12.44	63.93	27.54
	456.0	1.47	10.11	7.71	6.98	5.34	12.09	40.33	34.56
	480.0	1.81	16.29	11.20	9.83	7.31	9.15	22.94	41.06
	504.6	2.19	23.29	12.93	9.53	4.16	6.40	18.77	61.40
	528.4	2.54	35.27	11.95	4.86	0.66	4.19	6.52	117.45
	552.0	2.99	46.56	6.82	0.93	0.06	2.43	3.68	170.21
	576.6	3.32	50.45	0.71	0.03	0.01	0.89	0.24	222.28
	600.0	3.87	42.78	0.20	0.01	0.01	0.35	0.00	197.16
2	336.0	0.74	1.29	0.59	0.62	0.37	4.93	133.06	8.50
	360.2	0.88	3.05	2.51	2.49	1.95	8.78	108.54	24.52
	384.0	1.08	5.26	4.71	4.23	3.07	12.05	77.90	30.22
	408.0	1.38	8.57	7.05	5.90	3.87	13.66	43.57	35.08
	432.0	1.69	15.57	10.82	8.78	6.53	11.07	26.59	43.39
	456.0	2.09	23.12	14.33	11.51	7.84	8.57	21.44	49.90
	480.5	2.52	34.46	14.92	8.30	2.54	5.83	11.09	64.37
	504.2	2.99	44.04	8.03	1.64	0.32	3.81	4.16	85.33
	528.8	3.49	61.11	1.08	0.10	0.03	1.36	2.20	130.15
	552.1	3.89	59.85	0.22	0.02	0.01	0.45	0.12	157.04
	576.6	4.19	58.64	0.19	0.01	0.00	0.06	0.00	208.76
	600.9	4.45	52.80	0.16	0.00	0.00	0.07	0.00	203.78

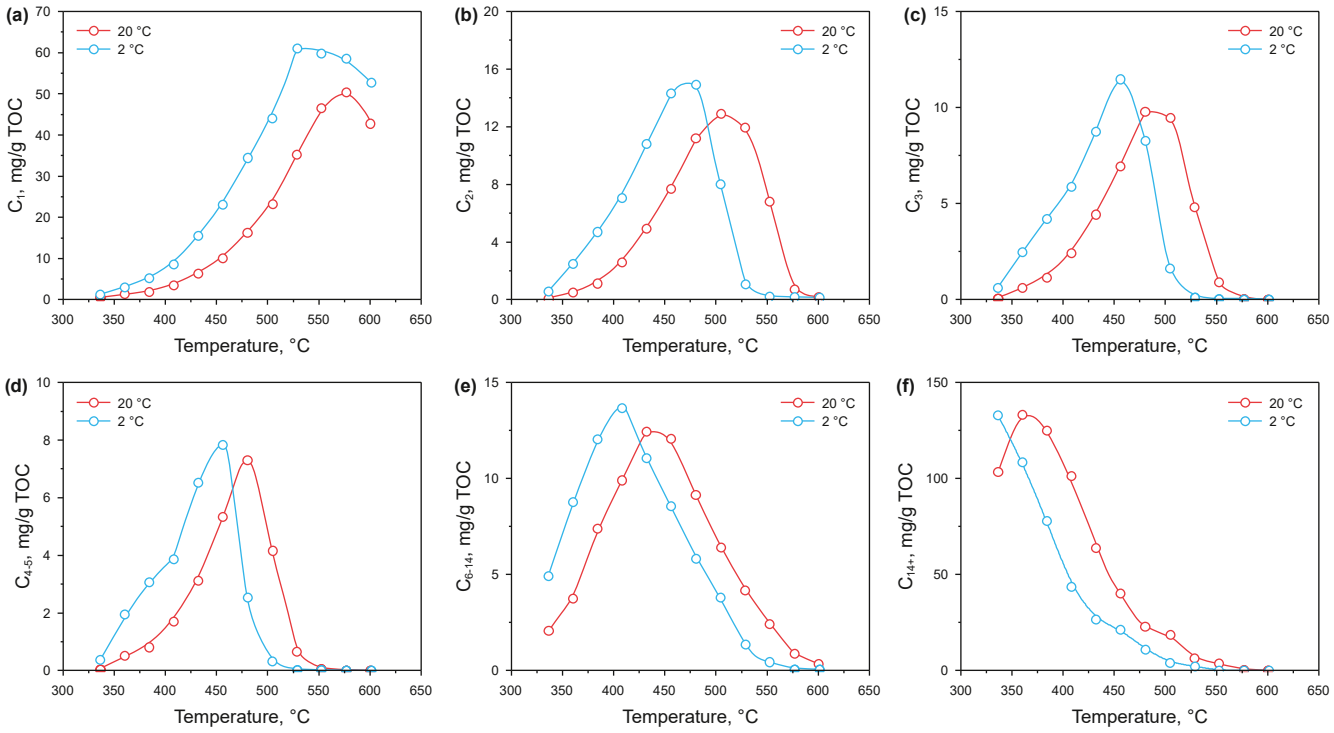

Fig. 4. Variation of hydrocarbon yields with increasing temperature in gold-tube pyrolysis experiments: (**a**) C_1; (**b**) C_2; (**c**) C_3; (**d**) C_{4-5}; (**e**) C_{6-14}; (**f**) C_{14+}.

(Tribovillard et al., 2009). Mineralogical data further support this interpretation, as pyrite occurs across most samples, serving as a typical indicator of a strongly reducing environment (Gu et al., 2025; Fakhraee et al., 2025). These characteristics indicate that the water body during the deposition of the E_3l was highly reducing, providing favorable conditions for the preservation of organic matter.

Carotane abundance provides evidence for salinity (Grba et al., 2014). Both γ-carotane and β-carotane are enriched, with γ-carotane dominant. Similar enrichment has been linked to saline reducing conditions in E_3l source rocks of the Linhe Depression, Hetao Basin (Zhang et al., 2025). Gammacerane, a marker of salinity and water column stratification, is present, and Gam/C_{30}H ratios confirm saline conditions (Holba et al., 2003; Peters et al.,

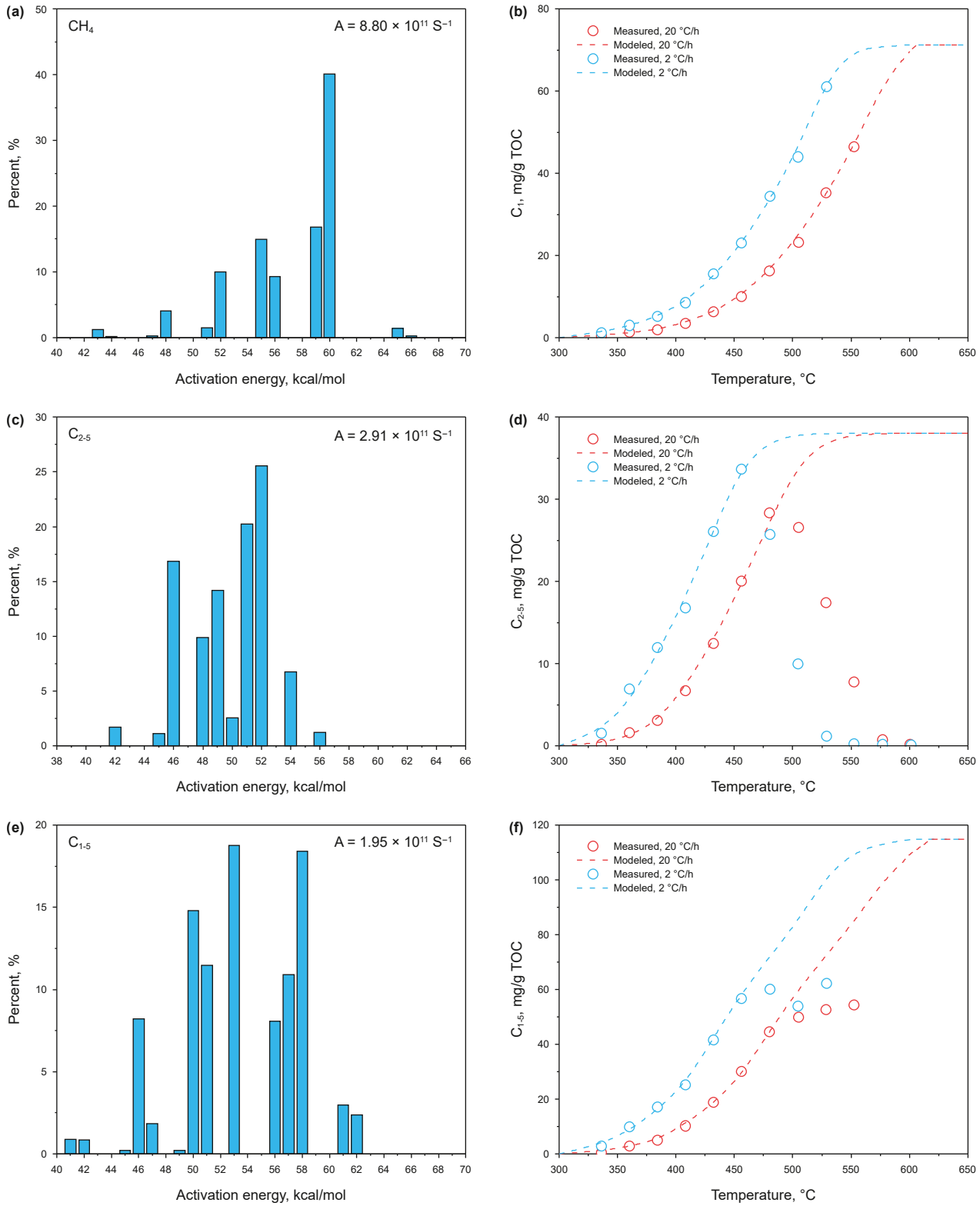

Fig. 5. Kinetic parameters, transformation ratio (TR) fitting curves and yield fitting curves of gaseous hydrocarbon. (**a**) Kinetic parameters of CH_4; (**b**) TR fitting curves of CH_4; (**c**) Kinetic parameters of $C_{2\text{-}5}$; (**d**) TR fitting curves of $C_{2\text{-}5}$; (**e**) Kinetic parameters of $C_{1\text{-}5}$; (**f**) TR fitting curves of $C_{1\text{-}5}$.

2005). The "upward tailing" distribution of C_{31}–C_{35} homohopanes is commonly observed in source rocks deposited in saline water environments (Haven et al., 1986). The majority of samples in the study area exhibit this feature, indicating deposition in a saline water environment (Figs. 3 and 10). Gam/C_{30}H ratio between 0.1 and 0.25 represents brackish water, 0.25–0.50 indicates saline water; 0.5–1.0 suggests highly saline water; and the value >1.0 signifies an extremely saline environment. Except for HT1, average Gam/C_{30}H values in all other samples exceed 0.50. The results suggest that the depositional water body was characterized by

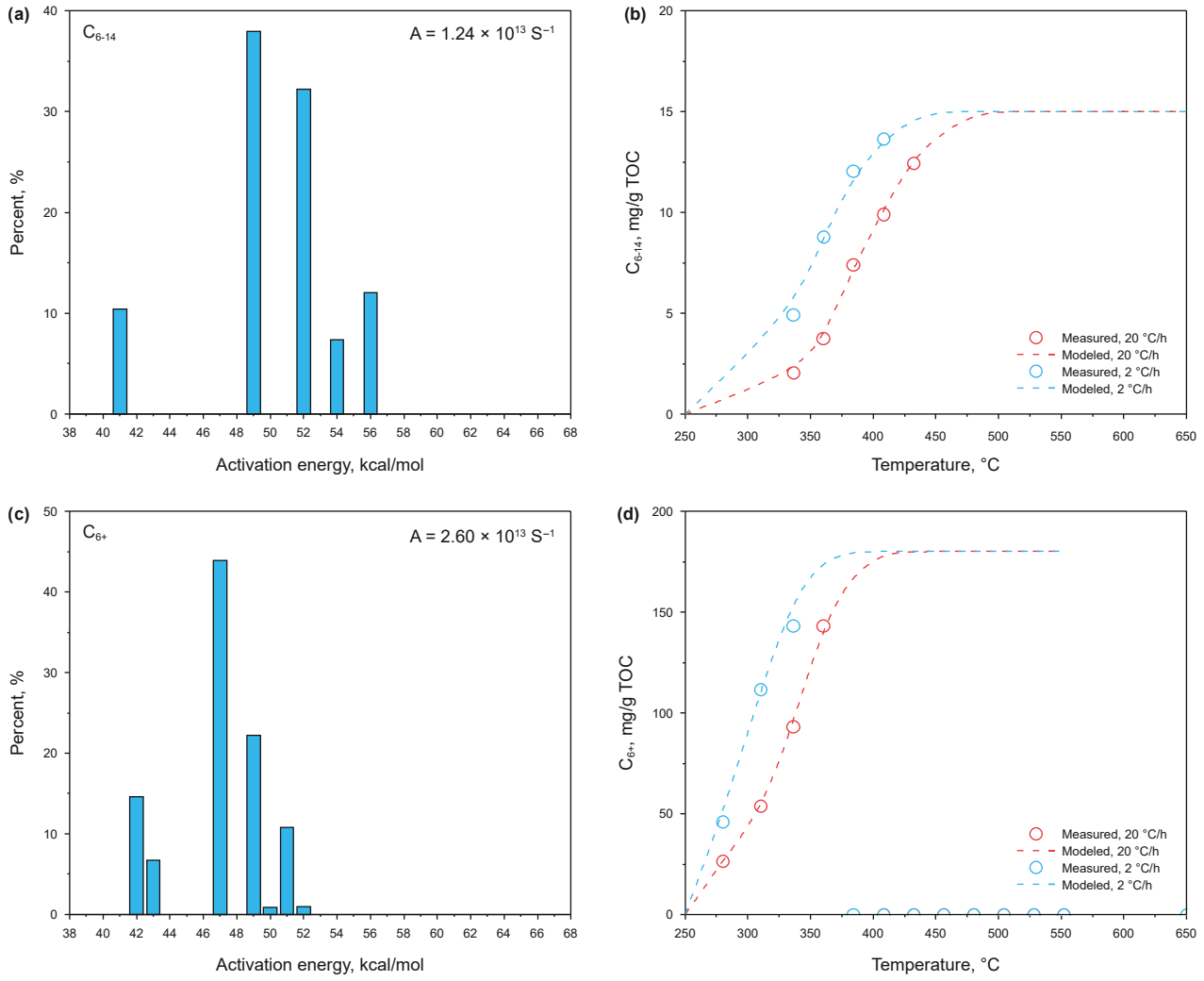

Fig. 6. Kinetic parameters, transformation ratio (TR) fitting curves and yield fitting curves of liquid hydrocarbon. (**a**) Kinetic parameters of $C_{6\text{-}14}$; (**b**) TR fitting curves of $C_{6\text{-}14}$; (**c**) Kinetic parameters of C_{6+}; (**d**) TR fitting curves of C_{6+}.

hypersaline-to-brine conditions (Fig. 9(b)). The detection of anhydrite and dolomite in samples from XH12-2 and LH1X further corroborates this conclusion (Table 2; Fig. 2) (Warren, 2006). The relationship between depositional water salinity and reducibility will be discussed in detail in Section 5.4.2.

5.3. Model of hydrocarbon generation evolution

The classic kerogen hydrocarbon generation model of Tissot and Welte (1984) defines four stages of oil and gas formation: biogenic methane ($R_o < 0.5\%$), oil generation ($0.5\% < R_o < 1.3\%$), condensate and wet gas ($1.3\% < R_o < 2.0\%$), and the dry gas ($R_o > 2.0\%$). Thermal simulation experiments indicate that saline lacustrine source rocks of the E_3l, Linhe Depression, Hetao Basin, evolve through four main stages (Fig. 11).

In the immature to low-maturity stage ($0.3\% < R_o < 0.6\%$), kerogen pyrolysis yields mainly oil with limited gas. During maturity ($0.6\% < R_o < 1.3\%$), kerogen cracking continues to produce oil, accompanied by minor gas (Fig. 11(b) and (c)). During this stage, the yield of C_{14+} increases rapidly, reaching its peak accumulative yield at around $R_o = 0.68\%$, while the accumulative yield of $C_{6\text{-}14}$ continues to grow and peaks at approximately $R_o = 1.3\%$ (Fig. 11(c)).

At high-maturity ($1.3\% < R_o < 2.0\%$), hydrocarbon generation shifts to oil cracking and kerogen degradation producing gas. Liquid hydrocarbon crack sequentially: C_{14+} converts to $C_{6\text{-}14}$, followed by $C_{6\text{-}14}$ cracking into gaseous hydrocarbons ($C_{1\text{-}5}$), primarily methane (Tang et al., 2009). When R_o reaches approximately 1.4%, the cumulative yield of wet gas increases rapidly, while the cumulative yield of C_{6+} begins to decline sharply, indicating that the cracking rate of liquid hydrocarbons now exceeds their generation rate, leading to a gradual reduction in liquid hydrocarbon content (Fig. 11(b) and (c)). At around $R_o = 1.8\%$, the cumulative yield of wet gas ($C_{2\text{-}5}$) peaks, while the cumulative yield of C_{6+} continues to decrease.

In the over-maturity stage ($R_o > 2.0\%$), kerogen generation yields primarily methane (C_1), with cumulative production rising but slowing (Fig. 11(b)). Residual C_{6+} and $C_{2\text{-}5}$ undergo further cracking, approaching depletion. Hydrocarbon generation potential diminishes markedly. Methane yield declines after $R_o \approx 3.25\%$, while the H_2S peaks, suggesting involvement of thermochemical sulfate reduction (TSR). The specific mechanism will be discussed in Section 5.5.2.

Crude oil in the study area is predominantly low-maturity oil (Fu et al., 2018; Wu et al., 2024), with peak hydrocarbon generation at $R_o = 0.68\%$, earlier than the peak at $R_o = 1.0\%$ in the classic

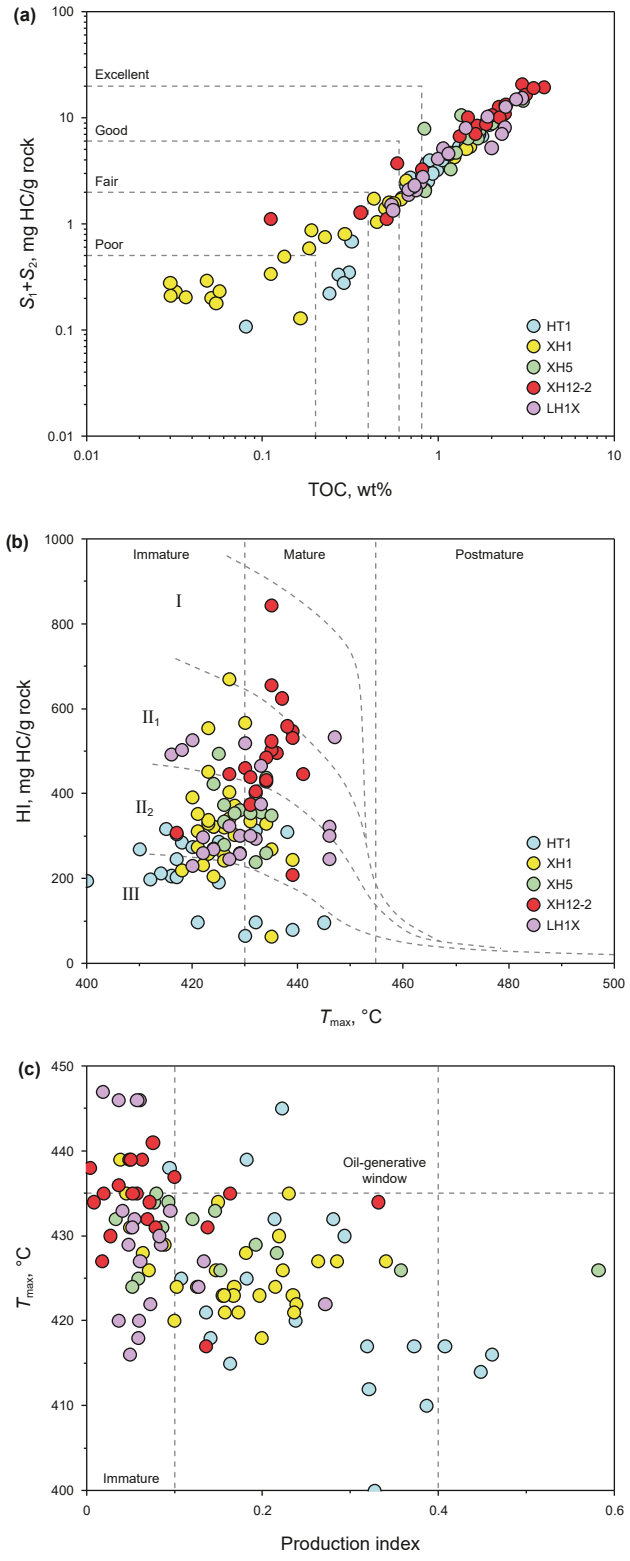

Fig. 7. Source rock evaluation. (**a**) TOC-S_1+S_2 (Peters and Moldowan, 1993); (**b**) T_{max}-HI (Tissot and Welte, 1984); (c) T_{max}-PI.

kerogen hydrocarbon generation model proposed by Tissot and Welte (1984). This indicates early hydrocarbon generation in source rock. Comparison with the Neogene Shanxi Formation freshwater source rocks (TOC = 2.63%) on the eastern Ordos Basin margin (He et al., 2022), shows that despite TOC values 2.5 times higher, hydrocarbon yields are similar. This further supports the view that source rocks in saline lacustrine basins exhibit higher hydrocarbon generation efficiency per unit of organic matter.

5.4. Causes of low TOC in source rocks

5.4.1. Salinity gradients control organic matter input by regulating biological productivity

Salinity during deposition exerts a major influence on biological development (Barbe et al., 1990; Warren, 2011). Biomarker-derived salinity indicator exhibit a parabolic relationship with TOC content, with TOC initially increasing and subsequently decreasing as salinity rises. Maximum TOC values occur when the Gam/C_{30}H ratio ranges from 0.6 to 1.0 and both γ-carotane index and β-carotane index approximate 0.01 (Fig. 12). The C_{27}–C_{29} regular sterane ternary diagram indicates that the organic matter is dominated by higher plants, supplemented by lower aquatic organisms (Fig. 13). Fu et al. (2025) reported the detection of green algae such as *Pediastrum* and *Botryococcus*, along with acritarchs like *Leiosphaeridia/Granomarginata*, in the source rocks of the study area. Simultaneously, a significant amount of Pinaceae pollen was also identified. Furthermore, Pinaceae pollen is rich in resinites (Jin et al., 1998).

Organic matter input from terrestrial higher plants remains relatively stable, whereas salinity primarily regulates the development of lower aquatic organisms. Saline environments enriched in nitrogen, phosphorus, and sulfur, provide nutrients supporting aquatic proliferation. Moreover, appropriate salinity levels can trigger blooms of halophilic organisms (Barbe et al., 1990; Warren, 2011), thus resulting in the formation of source rocks with relatively high TOC. However, excessively high salinity limits the diversity and abundance of lower aquatic organisms, leading to insufficient organic matter input and resulting in the development of low-TOC source rocks. When salinity is too low, although the diversity and abundance of organisms are high and organic matter input is substantial, the development of low TOC source rocks may still occur due to unfavorable preservation conditions. Thus, in low-salinity settings, preservation conditions rather than salinity dominate organic matter accumulation.

5.4.2. Salinity controls organic matter preservation conditions

Redox conditions during source rock deposition exert a primary control on organic matter preservation. Analysis of the depositional environment highlights the relationship between water salinity and reducibility. As shown in Fig. 14(a), the redox conditions become more reductive as the salinity of the depositional water body increases. Correspondingly, the TOC value gradually rises with the enhancement of reducibility (Fig. 14(b)).

Zones A, B, and C in Fig. 14(a) represent low, medium, and high salinity environments, respectively. Zone A receives adequate organic input; however, low salinity inhibits strongly reducing conditions, leading to poor preservation and low TOC. Zone B, characterized by moderate salinity, combines sufficient organic matter input and strong reducibility, promoting both the accumulation and preservation of organic matter, thereby yielding high-TOC source rocks. Zone C, despite having strong reducibility and favorable preservation conditions, experiences suppressed input of organic matter derived from lower aquatic organisms due to excessively high salinity, which also results in low TOC, even lower than that of Zone A (Fig. 14(b)).

5.4.3. Dilution and preservation of organic matter under tectonic-sedimentary coupling

As a Mesozoic-Cenozoic rift-superimposed basin, the Hetao Basin exhibits alternations of conglomerate, medium sandstone,

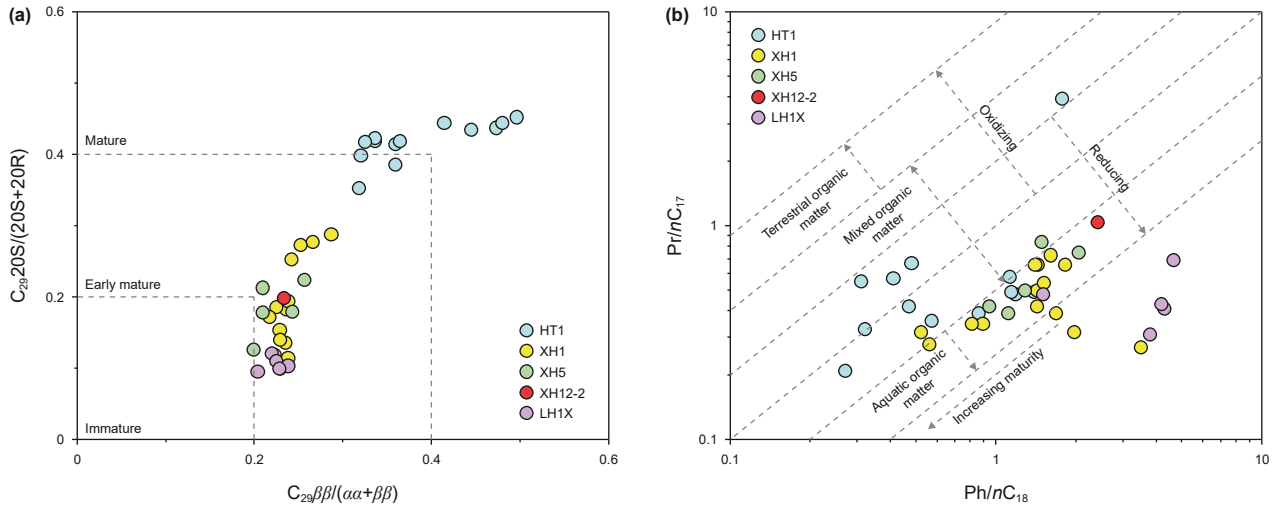

Fig. 8. Biomarker characteristics of E_3l source rock, Linhe Depression, Hetao Basin. (**a**) $C_{29}\beta\beta/(\alpha\alpha+\beta\beta)$-$C_{29}$20S/(20S + 20R) (Peters et al., 2005); (b) Ph/nC_{18}-Pr/nC_{17} (Tribovillard et al., 2009).

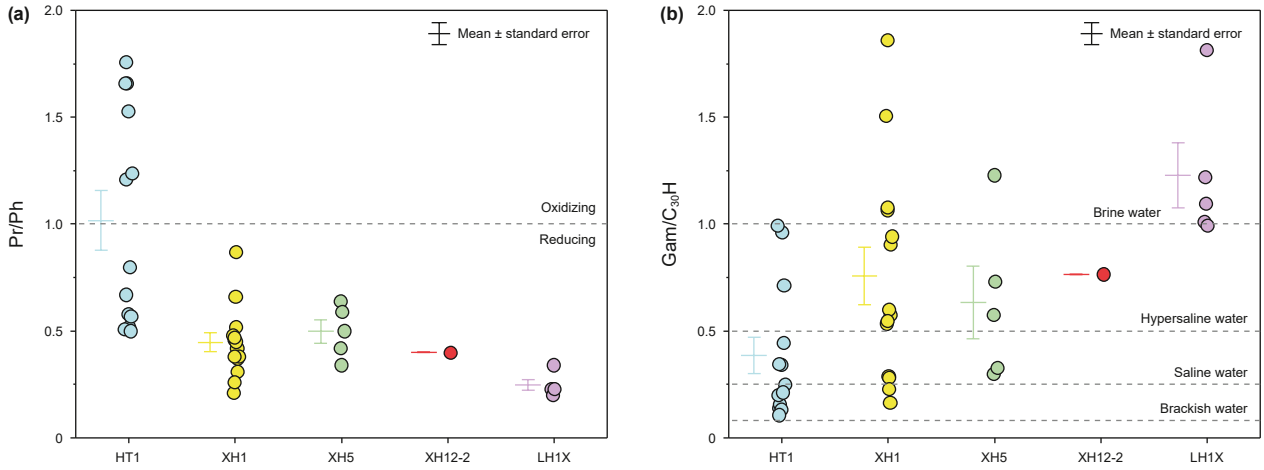

Fig. 9. Depositional environment characteristics of the E_3l source rocks, Linhe Depression, Hetao Basin. (**a**) Pr/Ph scatter plot; (**b**) Gam/C_{30}H scatter plot.

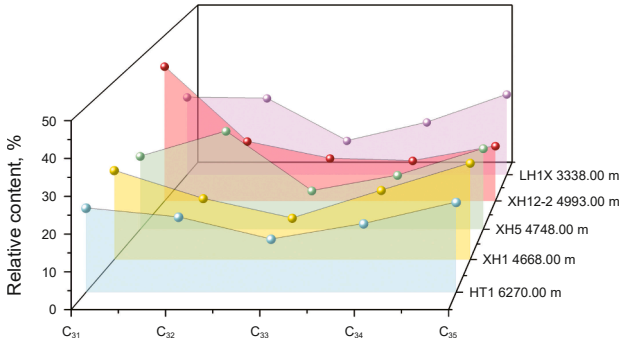

Fig. 10. Waterfall plot showing the relative content of homohopanes of E_3l source rocks, Linhe Depression, Hetao Basin.

and mudstone in the E_3l Formation reflecting proximal sourcing and rapid deposition (Fig. 1(d)). The rapid input of large amounts of terrigenous clastics filled the basin, significantly diluting the organic matter and resulting in its low content. The high proportions of clay minerals (average 47.62%) and quartz (average 21.57%) further indicate a continuous input of terrigenous clastics, with surrounding tectonic activities supplying abundant sediment sources. However, the strong dilution by evaporite minerals in the rapidly deposited clastic sediments confirms the dilution effect of inorganic minerals on organic matter.

Although geochemical indicators consistently suggest that the E_3l source rocks were deposited in a reducing environment, a high input of terrigenous clastics is also observed. This apparent contradiction is explained by the combined influence of sedimentation rate and water column stratification in a rapidly subsiding saline lake basin. Intense Oligocene subsidence in the Linhe Depression expanded accommodation space, enabling the accumulation of clastics from surrounding uplifts. High sedimentation rates promoted rapid burial of organic-rich sediments, minimizing exposure at the oxic interface and isolating organic matter. Concurrently, salinity-driven stratification inhibited vertical mixing, maintaining anoxic bottom waters. Even with oxygenated surface inflow, sediment particles bypassed the surface layer and settled in the anoxic zone, reinforcing bottom water isolation. Thus, terrigenous input occurred not in a dynamic oxic setting, but within a stratified saline lake basin with a stable structure. The intense clastic input coupled with rapid burial coexisted and interacted spatiotemporally with the strongly reducing conditions

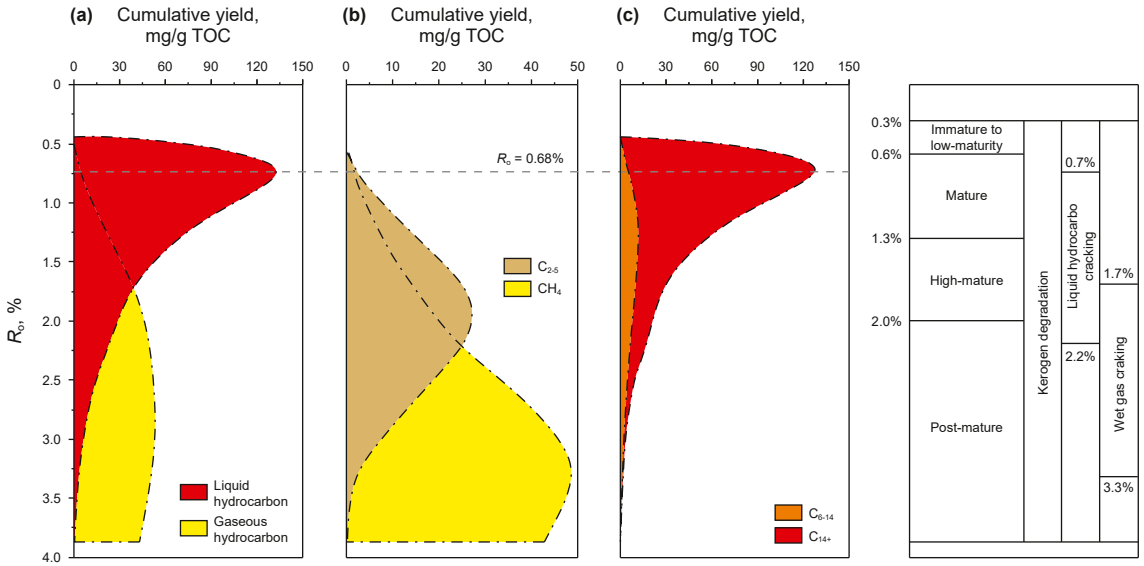

Fig. 11. Hydrocarbon generation model of low-TOC source rocks, Linhe Depression, Hetao Basin. (**a**) Evolution profiles of gaseous and liquid hydrocarbon generation; (**b**) Evolution profiles of CH_4 and C_{2-5} generation; (**c**) Evolution profiles of C_{6-14} and C_{14+} generation.

induced by salinity stratification, jointly constituting the key to the high preservation efficiency of the E_3l source rocks.

In summary, the low-TOC source rocks in the study area reflect the combined influence of tectonic and depositional processes. Intense rifting activities generated steep paleo-topography and elevated sedimentation rates, producing a significant dilution of organic matter by terrigenous clastics. The tectonic paleogeography formed a semi-closed to closed basin, where arid climatic conditions resulted in water salinization and salinity stratification. This created a reducing lacustrine bottom environment conducive to organic matter preservation. Additionally, saline water conditions favored specialized biota such as halophilic algae, forming high-quality source rocks with substantial hydrocarbon generation potential.

Therefore, the low TOC in the Hetao Basin does not indicate low productivity or poor preservation conditions. Rather, it reflects a specific source rock type formed under high sedimentation rates, with preservation efficiency enhanced by salinity stratification. Its resource potential stems not only from organic matter abundance but also benefits from high conversion efficiency and hydrocarbon expulsion efficiency, which will be discussed further in subsequent sections.

5.5. Causes of low TOC in source rocks

5.5.1. Key to high hydrocarbon generation efficiency: low activation energy and high frequency factor

Kinetic parameters derived from thermal simulation experiments provide critical evidence for high hydrocarbon generation potential under low-TOC conditions. The dominant activation energy peak for C_{6+} is only 47 kcal/mol, accompanied by the highest frequency factor among all components, indicating a high reaction attempt frequency. Once the activation threshold is reached, kerogen conversion proceeds rapidly, yielding substantial liquid hydrocarbons at relatively low temperatures (shallow burial depths), thereby explaining early hydrocarbon generation. Compared to the Qianjiang Formation source rocks in the Jianghan Basin, which have a primary peak activation energy for C_{6+} of 54 kcal/mol (Wang et al., 2020), and the Lucaogou Formation source rocks in the Junggar Basin with an activation energy for C_{6+} of 50 kcal/mol (Xiang et al., 2016), this comparison highlights that the E_3l source rocks exhibit significantly lower hydrocarbon generation activation energy, reflecting a reduced generation threshold and enhanced efficiency.

Low activation energy is typically associated with hydrogen-rich chemical bonds derived from aliphatic chain structures derived from sources such as lipids and algae (Bertrand et al., 1986). Halophilic algae and bacteria that thrive in saline lacustrine basins are rich in lipids and lipid-like compounds, making them high-quality oil-prone precursors. Fu et al. (2025) not only detected algae and Pinaceae pollen but also conducted maceral separation on the same samples used in the thermal simulation experiments of this study, isolating hydrogen-rich hydrocarbon-generating components such as resinite, sporinite, alginite, and desmocollinite. Among these, resinite exhibits the highest hydrocarbon generation potential (S_2 = 94.35 mg/g) and hydrogen index (HI = 508.33 mg HC/g TOC), along with the lowest activation energy (53.3–56.2 kcal/mol). It demonstrates a two-stage hydrocarbon generation pattern, contributing up to 40% of the total generated hydrocarbons, second only to alginite. Its peak hydrocarbon generation occurs at $R_o \approx 0.61\%$, which is consistent with the hydrocarbon generation model established in this study ($R_o = 0.68\%$) (Fig. 11). Resinite is primarily derived from Pinaceae, a family of terrestrial higher plants. Combined with Fig. 12, the results demonstrate that the organic matter in the E_3l source rocks of the study area is predominantly derived from higher plants, with contributions from lower aquatic organisms such as algae. This indicates that the low-activation-energy oil-prone precursors are mainly composed of resinite supplied by higher plants and alginite provided by lower aquatic organisms.

5.5.2. Positive feedback mechanism of TSR-H_2S-catalyzed hydrocarbon generation

Thermochemical Sulfate Reduction (TSR) is a redox process in which hydrocarbons react with solid sulfate minerals under high-temperature anaerobic conditions, producing H_2S, carbonates, and releasing heat and CO_2 (Machel, 2001; Meshoulam et al., 2016; Zhang et al., 2007). The E_3l source rocks contain abundant anhydrite, providing ample sulfate sources for TSR (Fig. 2). Burial depths exceeding 3000 m, satisfying the geothermal conditions

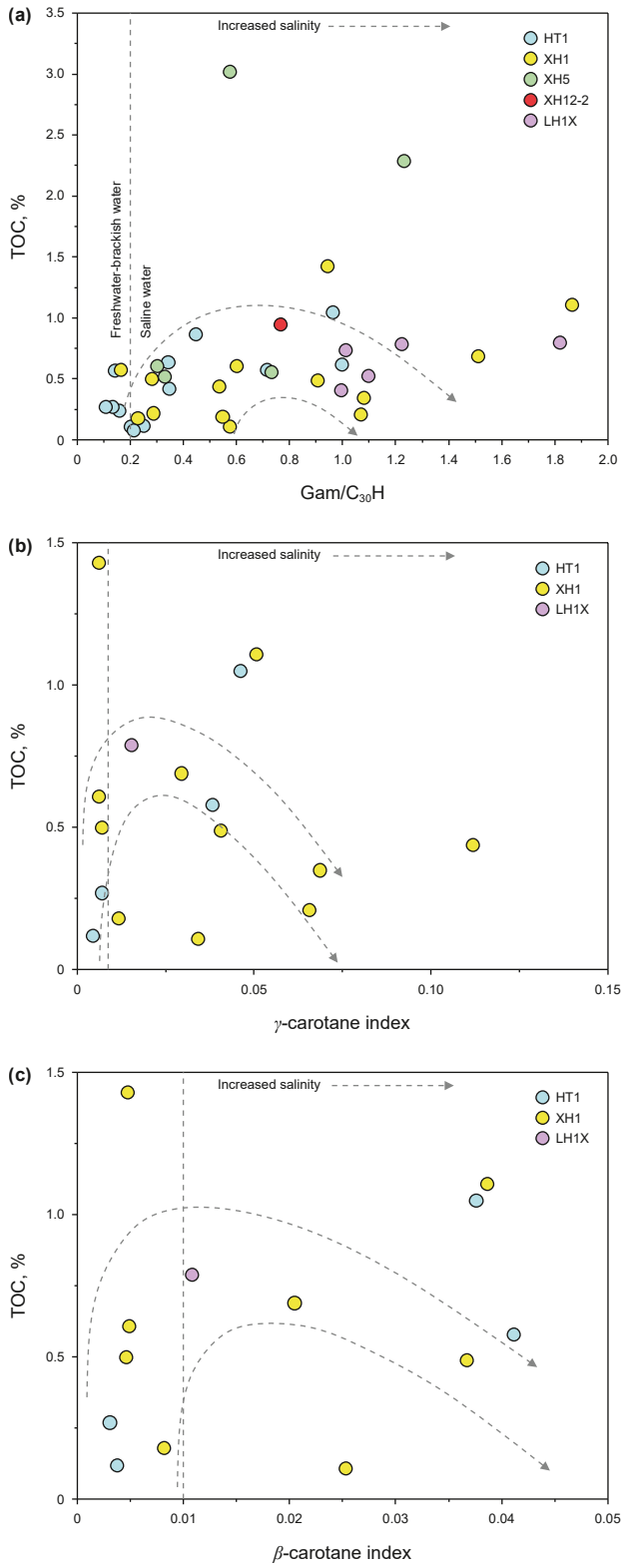

Fig. 12. Relationship between biomarker salinity indicators and TOC of E_3l source rocks, Linhe Depression, Hetao Basin. (**a**) Gam/C_{30}H vs. TOC; (**b**) γ-carotane index vs. TOC; (**c**) β-carotane index vs. TOC.

required for TSR reactions, leading to extensive TSR reactions during hydrocarbon generation in the E_3l source rocks.

The sulfate ion (SO_4^{2-}) is chemically stable and requires high temperatures for activation. The small amount of H_2S generated at

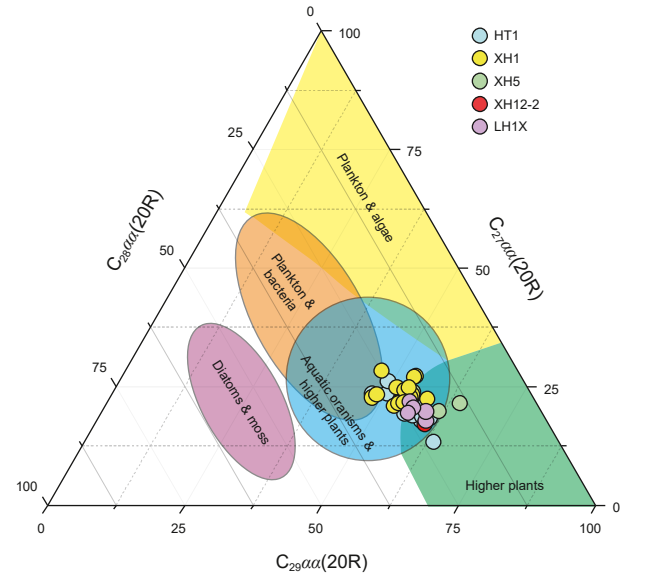

Fig. 13. Ternary diagram of C_{27}, C_{28}, and C_{29} regular steranes for E_3l source rocks, Linhe Depression, Hetao Basin (Peters et al., 2005).

low temperatures may originate from the cracking of sulfur-containing organic matter. As the temperature increases, the TSR chain reaction initiates, where SO_4^{2-} reacts with H_2S to form unstable, highly reactive oxidants such as SO_3^{2-} and S (Eq. (1)).

$$SO_4^{2-} + H_2S \xrightarrow{\Delta} SO_3^{2-} + S + H_2O \quad (1)$$

When the simulation temperature exceeds 500 °C, the highly reactive oxidants (SO_3^{2-} and S) generated in Eq. (1) rapidly react with hydrocarbon molecules (using CH_4 as an example, Eqs. (2) and (3)). This process simultaneously produces a large amount of H_2S, which further reacts with sulfate minerals, continuously generating SO_3^{2-} and S, thereby forming an autocatalytic cycle. This leads to a sharp increase in H_2S concentration, indicating that the TSR reaction has entered a dominant stage (Fig. 15).

$$CH_4 + SO_3^{2-} + 2H^+ \xrightarrow{\Delta} CO_2 + H_2S + 2H_2O \quad (2)$$

$$CH_4 + 2S + 2H_2O \xrightarrow{\Delta} CO_2 + 2H_2S \quad (3)$$

Fig. 15 elucidates the positive feedback cycle mechanism of TSR-H_2S-catalyzed hydrocarbon generation at 500–600 °C. Based on kinetic principles, the short-term, high-temperature thermal simulation in the experiment corresponds to the long-term, low-temperature evolution process in geological history. Using EasyR_o as a unified maturity scale, a significant surge in H_2S yield is observed approximately after EasyR_o > 2.0% (Table 5). Combined with the geothermal gradient of the study area (2.6 °C/100 m), this maturity threshold roughly corresponds to a burial depth exceeding 5000 m. At this stage, peak oil generation has passed, and a substantial amount of early-formed liquid hydrocarbons have undergone cracking, allowing the initial concentration of H_2S in the formation to accumulate to a critical level, thereby activating and intensifying the TSR chain reaction. Therefore, this study infers that the TSR-H_2S positive feedback mechanism represents a critical efficiency-enhancing process in hydrocarbon generation within deep petroleum system of the Linhe Depression, particularly for the formation of oil-cracking gas and late-stage kerogen-cracking gas.

Although TSR reactions consume a portion of hydrocarbons, the generated H_2S and its derived sulfur radicals (S·) act as highly

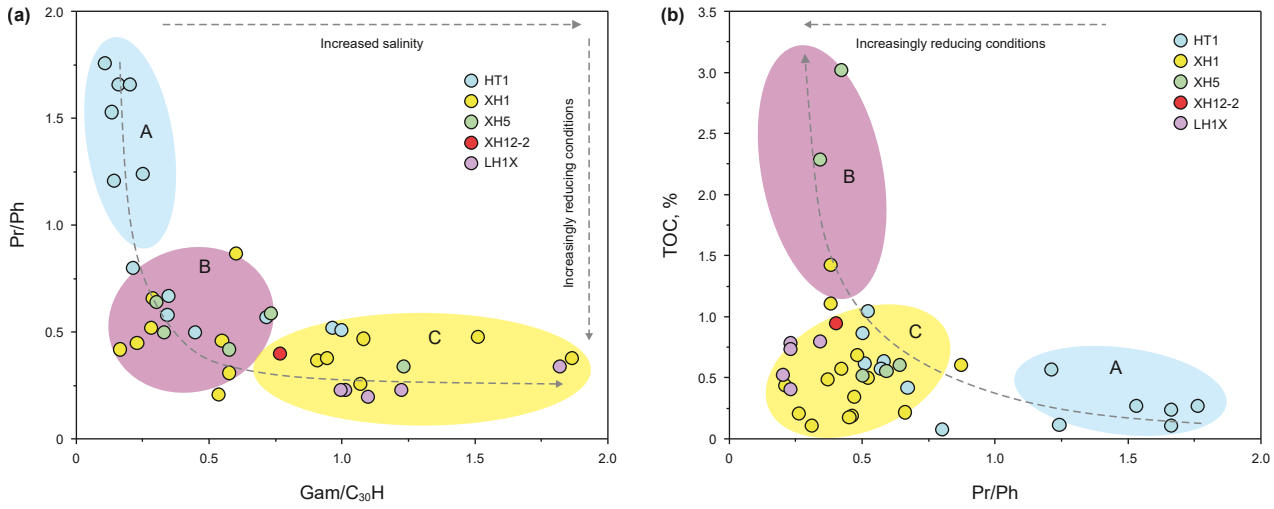

Fig. 14. Analysis of organic matter preservation conditions in E_3l source rocks, Linhe Depression, Hetao Basin. (**a**) Gam/C_{30}H-Pr/Ph; (**b**) Pr/Ph-TOC.

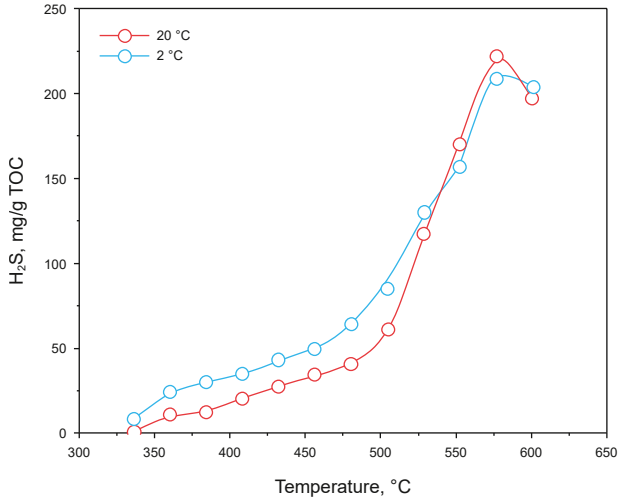

Fig. 15. Variation of H_2S with increasing temperature in gold-tube pyrolysis experiments.

efficient catalysts. These H_2S immediately catalyze the hydrocarbon generation from the remaining kerogen and the cracking of liquid hydrocarbons. Sulfur radicals attack C–C and C–H bonds, significantly reducing the activation energy required for oil cracking to gas and late-stage kerogen degradation, thereby triggering an "explosive" generation of gaseous hydrocarbons (Fig. 11(b)). The consumption and regeneration of H_2S during the reaction form a self-enhancing catalytic cycle, markedly improving organic matter conversion efficiency. This process enables the E_3l source rocks to generate substantial volumes of oil and gas, providing a reasonable explanation for the origin of the high resource potential. This series of reactions constitutes a positive feedback mechanism of TSR-H_2S-catalyzed hydrocarbon generation.

5.5.3. *Mineral catalysis: catalytic effects of illite/smectite mixed-layer clay (I/S), pyrite, gypsum, and carbonate minerals*

The mineral assemblages developed in the study area exhibit catalytic activity that enhances hydrocarbon generation efficiency despite low TOC. Illite/smectite mixed-layer clay (I/S) exhibits acid catalysis, wherein Brønsted acid sites (H^+) and Lewis's acid sites (Al^{3+}) on its surface can significantly reduce the activation energy required for kerogen thermal degradation and crude oil cracking via the formation of carbocation intermediates. This promotes hydrocarbon generation at lower maturity levels and higher rates, effectively catalyzing the cleavage of C–C and C–O bonds (Hu et al., 2014; Ola et al., 2018). Clay mineral content is relatively high (average 47.62%), with I/S being the most abundant component (average 74.27%) (Table 2). This indicates highly favorable catalytic conditions. I/S enhances hydrocarbon generation potential by reducing activation energy: under similar Tmax conditions, the hydrocarbon generation potential increases with higher I/S content (Fig. 16(a)). This indicates that after undergoing similar thermal evolution, source rocks rich in I/S retained more hydrogen or consumed less hydrogen during hydrocarbon generation, resulting in higher effective hydrogen content. This directly demonstrates that I/S catalysis enhances hydrocarbon generation efficiency and preserves hydrocarbon generation potential. Moreover, under comparable TOC conditions, S_1+S_2 increases with rising I/S content (Fig. 16(b)), further indicating that similar amounts of organic matter yield different hydrocarbon generation quantities due to variations in catalyst concentration. Samples with higher I/S content exhibit greater conversion rates, confirming the catalytic enhancement effect on hydrocarbon generation. Notably, it is important to highlight that although a positive correlation exists overall between I/S and hydrocarbon generation parameters, inter-well variations are still observed. This key point reveals that, besides mineral catalysis, the quality and type of organic matter remain the primary foundation controlling hydrocarbon generation potential. Mineral catalysis serves only as an enhancement mechanism on this basis.

In addition to serving as a reactant in TSR, anhydrite, with its high thermal conductivity, facilitates the transfer of deep heat to the overlying source rocks, thereby promoting hydrocarbon generation (Bao et al., 2023; Fu et al., 2025; Meng et al., 2022; Xia et al., 2014). During thermal evolution, pyrite decomposes to produce reactive sulfur radicals (S·), which attack C–H bonds to generate highly reactive hydrogen radicals. These radicals initiate and accelerate free radical cracking reactions, significantly enhancing the rate of hydrocarbon generation. Although the pyrite content in the study area is relatively low (average 4.39%), its catalytic efficiency is exceptionally high (Lewan, 1998; Lewan and Ruble, 2002). Carbonate minerals (with a combined calcite and dolomite content of 18.29%), though exhibiting relatively weak catalytic capacity, create alkaline microenvironments that may promote

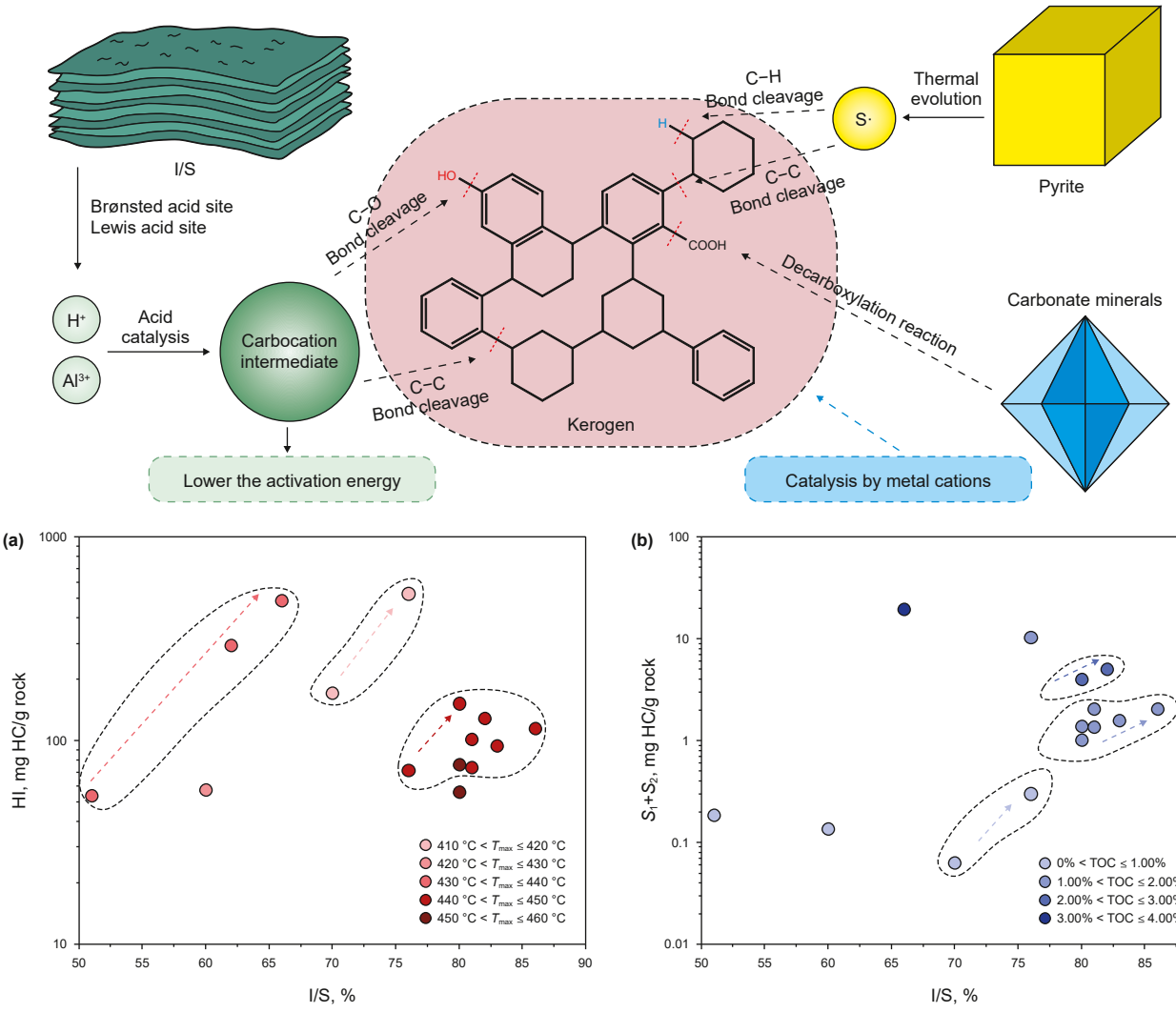

Fig. 16. Model of mineral-catalyzed hydrocarbon generation. (**a**) I/S-HI; (**b**) I/S-S_1+S_2.

decarboxylation reactions, providing supplementary pathways for hydrocarbon generation (Akira and William, 1972).

5.5.4. Potential synergistic effects between mineral catalysis and the TSR process

This study identifies that mineral catalysis and the TSR-H_2S positive feedback cycle are key drivers of efficient hydrocarbon generation in the E_3l source rocks of the Linhe Depression. Based on existing data and the discussions above, a conceptual model of "two-step relay catalysis" is proposed, where each mechanism dominates different stages of hydrocarbon evolution and may act synergistically.

In the early to middle stage (R_o < 1.3%), kerogen thermal degradation and crude oil cracking are the primary pathways for hydrocarbon generation (Fig. 11). The abundant I/S and pyrite in the study area play the main catalytic roles at this stage. The acid sites in I/S promote C–C bond cleavage (Hu et al., 2014; Ola et al., 2018), while the redox activity of pyrite may be involved in the preliminary activation of sulfur. These processes not only generate hydrocarbons directly but may also produce some active sulfur species, laying the groundwork for the initiation of deep-seated TSR.

When the source rocks enter a deep, high-temperature environment (R_o > 2.0%), TSR reactions are activated, and H_2S and sulfur radicals become the dominant catalytic agents, establishing a robust autocatalytic cycle. During this stage, mineral catalytic processes transition to a synergistic role. Pyrite surfaces can act as stabilizers for sulfur radicals, lowering their binding energy and extending their catalytic lifetime (Adsul et al., 2025; Ding et al., 2016; Ma et al., 2016). Concurrently, the acidic fluids generated by TSR may, in turn, promote the transformation of clay minerals like I/S, continuously releasing interlayer ions to maintain catalytic activity (Hu et al., 2014; Ola et al., 2018). This interaction between mineral surfaces and fluid-borne radicals may constitute a composite catalytic system that is more efficient and stable than either a pure aqueous-phase TSR or mineral catalysis alone.

5.5.5. Formation overpressure: inhibiting cracking and promoting expulsion

With increasing burial depth and geothermal temperature, liquid hydrocarbons typically undergo conversion to gaseous hydrocarbons (Tissot and Welte, 1984). The study area is dominated by light oil even in ultra-deep strata, indicating favorable preservation of liquid hydrocarbons. This is primarily due to the unique preservation mechanism for liquid hydrocarbons under formation overpressure conditions. As a rapidly subsiding rift basin, the Linhe Depression is prone to developing overpressure systems. For instance, in Well HT1, the formation pressure

coefficient reaches as high as 1.54 (Wu et al., 2024), creating an excellent closed-system environment for the preservation of liquid hydrocarbons.

Overpressure alters the phase state and chemical equilibrium of hydrocarbon reactions: on the one hand, it inhibits the secondary cracking of liquid hydrocarbons by increasing the activation energy of cracking reactions, thereby delaying the breakage of C–C bonds and slowing down the conversion rate of crude oil to natural gas through cracking. This provides a crucial kinetic barrier for the long-term stable preservation of liquid hydrocarbons in high-temperature, deep subsurface environments; on the other hand, over pressured systems typically exhibit low permeability. Such a relatively closed physicochemical environment suppresses the progression of catalytic cracking reactions, further protecting the already generated liquid hydrocarbons.

Overpressure also influences hydrocarbon migration efficiency. Although the E_3l source rocks have relatively low TOC, their intense hydrocarbon generation itself is a major contributor to overpressure. The Linhe Depression has undergone rapid subsidence since 5.3 Ma, causing the source rocks to reach the peak hydrocarbon generation window within a short period. This "explosive" hydrocarbon generation led to a sharp increase in fluid pressure, creating a significant source–reservoir pressure difference (Wu et al., 2024). Diagenetic physical experiments indicate that when overpressure exceeds the rock fracture pressure, it can generate extensive microfracture systems within the source rocks and adjacent sandstones. These microfractures provide efficient migration pathways for oil and gas, enabling episodic hydrocarbon expulsion and significantly improving expulsion efficiency (Jin et al., 2023).

Therefore, formation overpressure plays a dual role in the hydrocarbon accumulation process of low-TOC source rocks in the study area: it not only serves as a key condition for inhibiting liquid hydrocarbon cracking and enabling efficient preservation, but also acts as the core driving force behind the formation of micro-fractures and the promotion of episodic, efficient hydrocarbon expulsion. This complete dynamic process can be summarized as the mechanism of generation, migration, and preservation of liquid hydrocarbons driven by formation overpressure (Fig. 17). This mechanism ensures that under a low-TOC background, the generated hydrocarbons can be effectively preserved, efficiently migrated, and accumulated, ultimately forming petroleum accumulations with high resource potential.

5.6. Universality and specificity of hydrocarbon generation in the saline Linhe Formation

This study examines Oligocene saline lacustrine source rocks in the Linhe Depression, highlighting their efficient hydrocarbon generation despite low-TOC. Unlike the classical model, which emphasizes abundant organic matter and favorable preservation conditions (Tissot and Welte, 1984), this study demonstrates that in saline lacustrine basins, significant source rocks can also form even with initially low TOC, provided there is excellent preservation combined with efficient catalysis and expulsion mechanisms. This insight challenges existing research boundaries.

Terrestrial saline lacustrine source rocks in China are primarily categorized into sulfate-type and alkaline-type. Sulfate-type saline lacustrine basins mainly include the Lower Ganchaigou Formation in the Qaidam Basin, the Qianjiang Formation in the Jianghan Basin, and the Shahejie Formation in the Bohai Bay Basin. Alkaline-type lakes are represented by the Fengcheng and Lucaogou Formations in the Junggar Basin (Liang et al., 2024; Tang et al., 2021a,b; Xia et al., 2024). Currently, research on hydrocarbon generation in China's terrestrial saline lacustrine source rocks remains limited, with most studies primarily concentrated on alkaline-type deposits in the Junggar Basin and the Lower Ganchaigou Formation of the Qaidam Basin (Cao et al., 2025; Li et al., 2023).

The Fengcheng Formation in the Junggar Basin is a typical alkaline-type source rock, characterized by high pH, abundant carbonate minerals, and alkaline minerals (Wang et al., 2020; Yu et al., 2018). The developed Botryococcusand cyanobacteria provide the material basis for its bimodal hydrocarbon generation. Unique alkaline minerals and volcanic minerals respectively delay and advance the peak oil generation stage, altering the hydrocarbon generation process. This reflects the synergistic evolution of biology and environment, as well as organic-inorganic interactions. Furthermore, tectonic uplift promoted bimodal hydrocarbon generation (Cao et al., 2025). The TOC values of the Lower Ganchaigou Formation source rocks in the Qaidam Basin are generally low, primarily due to the saline environment, rapid deposition, and efficient conversion of hydrogen-rich organic matter. The organic matter is mainly derived from aquatic organisms and formed in a strongly reducing environment. Hydrocarbon generation kinetics indicates two pathways: early generation from soluble organic matter and later from kerogen, with the peak oil

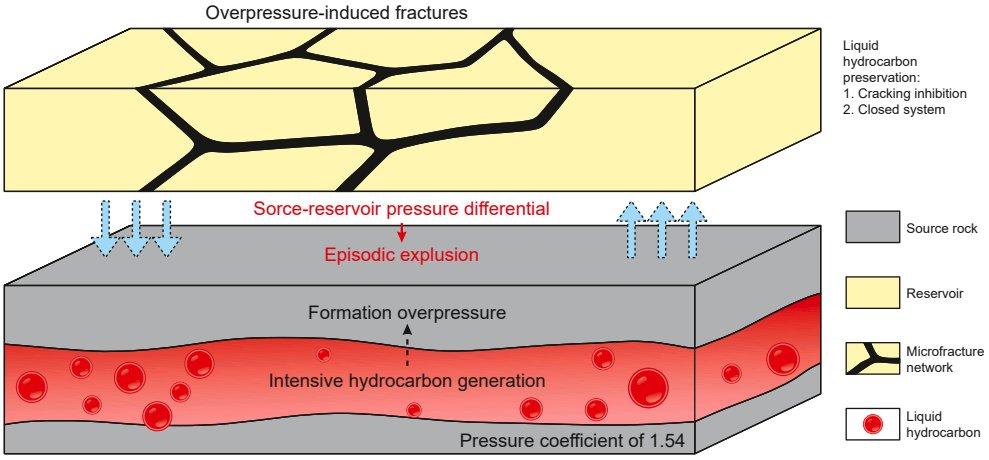

Fig. 17. Conceptual model of liquid hydrocarbon generation, migration, and preservation mechanisms driven by formation overpressure.

output at R_o value of approximately 1.0% (Li et al., 2023). While the Qaidam Basin also exhibits low TOC yet high resource potential, in-depth exploration from perspectives such as mineral catalysis and TSR reactions has not yet been conducted.

The Linhe Formation offers broad insights into hydrocarbon generation in saline lacustrine source rocks. Despite low TOC, such rocks show high generation potential, underscoring the importance of efficiency over abundance. Hydrocarbon output is shaped not only by organic matter but also by interaction with organic minerals, which is a universal process across sedimentary basins. The specificity of the Linhe Formation, distinguishing it from other saline lacustrine source rocks, lies in its unique mineral assemblage of I/S and anhydrite. This mineral combination is the key to forming the unique kinetic characteristics of low activation energy and high frequency factor, serving as the material basis for efficient hydrocarbon generation. The TSR-H_2S positive feedback cycle mechanism significantly enhances hydrocarbon yields, representing an important advancement in the understanding of hydrocarbon generation mechanisms in saline lacustrine basins. More importantly, this efficient hydrocarbon generation mechanism also depends on the specific sedimentary-tectonic setting of the Hetao Basin, a unique condition difficult to replicate in other basins. In summary, the study's universality lies in reframing evaluation towards efficiency, while its specificity rests on the Hetao Basin's singular geology and reaction pathways that create an exceptional, high-efficiency generation pathway.

6. Conclusion

Hydrocarbon generation in the Oligocene Linhe Formation (E_3l) source rocks of the Linhe Depression, Hatao Basin: A typical "hydrocarbon generation paradox". The Oligocene Linhe Formation (E_3l) source rocks in the Linhe Depression, Hetao Basin, exemplify a "hydrocarbon generation paradox," characterized by low TOC content (average 1.15%) yet high hydrocarbon generation potential. This paradox originates from a distinctive depositional environment. Geochemical proxies (Pr/Ph, Gam/$C_{30}H$ and Carotane index), and minerals such as anhydrite and pyrite indicate formation under a closed, stratified, hypersaline, and strongly reducing environment, which favored organic matter preservation.

Low TOC reflects the interplay of multiple factors within a coupled tectonic-sedimentary background. Moderate salinity supported moderate paleo productivity, while salinity stratification ensured strongly reducing preservation. Conversely, rapid subsidence induced high sedimentation rates and substantial terrigenous input, diluting organic matter.

Hydrocarbon generation kinetics demonstrates "early and efficient" conversion, with activation energy for the C_{6+} component as low as 47 kcal/mol and peak generation occurring at $R_o \approx 0.68\%$. This is attributed to the low activation energy characteristics of hydrogen-rich precursors like resinite and alginite.

The key mechanisms driving this efficient hydrocarbon generation are threefold: 1) A natural catalytic system of illite/smectite mixed-layer clay, pyrite, and anhydrite reduced activation energy. 2) H_2S and sulfur radicals form deep thermochemical sulfate reduction (TSR) established an autocatalytic cycle, enhancing hydrocarbon cracking. 3) Formation overpressure inhibited the secondary cracking of liquid hydrocarbons and, facilitated by a micro-fracture system, promoted episodic hydrocarbon expulsion and effective migration.

Overall, the sequence from precursor preservation to efficient conversion and expulsion confirms that "hydrocarbon generation efficiency" constitutes the core criterion for evaluating source rocks with low TOC but high hydrocarbon potential.

CRediT authorship contribution statement

Man Yuan: Writing – review & editing, Writing – original draft, Visualization, Methodology. **Jun-Gang Lu:** Writing – review & editing. **Shu-Guang Chen:** Data curation. **Yu-Lei Shi:** Data curation. **Ran-Ran Zhou:** Data curation. **Yi-Ming Fan:** Investigation. **Ying-Xuan Lyu:** Investigation. **Yi-Nuo Chen:** Visualization. **Ming Li:** Data curation.

Declaration of competing interest

The authors declare that they have no known competing financial interests or personal relationships that could have appeared to influence the work reported in this paper.

Acknowledgements

We thank the reviewers and the editorial office for their valuable comments. The samples used in this study were provided by PetroChina Huabei Oilfield Company, and the experimental measurements were supported by the State Key Laboratory of Oil and Gas Reservoir Geology and Exploitation and the Experimental Center of PetroChina Huabei Oilfield Company. This work was supported by the National Natural Science Foundation of China (Grant No. 42072185) and the Sichuan Provincial Natural Science Foundation (Grant No. 2025ZNSFSC0309).

Nomenclature

E_3l	Linhe Formation
TOC	Total organic carbon
K_1g	Guyang Formation
Qtz	Quartz
Kfs	K-Feldspar
Plg	Plgioclase
Cal	Calcite
Dol	Dolomite
Py	Pyrite
Anh	Anhydrite
Anl	Analcime
Kln	Kaolinite
PI	Production index
T_{max}	Temperature with maximum hydrocarbon generation
S_1+S_2	Generative potential
Pr	Pristane
Ph	Phytane
Gam/$C_{30}H$	Gammacerane/C_{30} hopane
TSR	Thermochemical sulfate reduction
I/S	I/S mixed-layer
HI	Hydrogen index
Chl	Chiorite
Ill	Illite

References

Abdi, Z., Rimmer, S.M., 2024. Organic petrology and geochemistry of the Devonian-Mississippian bakken Formation, Williston Basin, North Dakota. Int. J. Coal Geol. 282, 104420. https://doi.org/10.1016/j.coal.2023.104420.

Adsul, T., Hackley, C.P., Hatcherian, J.J., et al., 2025. Reaction kinetics and accelerant effects of sulfides in early mature hydrocarbon generation using hydrous pyrolysis. J. Anal. Appl. Pyrolysis 192, 107307. https://doi.org/10.1016/J.JAAP.2025.107307.

Akira, S., William, D., 1972. Formation of alkanes from fatty acids in the presence of $CaCO_3$. Geochem. Cosmochim. Acta 36 (1), 87–91. https://doi.org/10.1016/0016-7037(72)90122-6.

Bao, H.P., Wang, Q.P., Yan, W., et al., 2023. Sedimentary characteristics and gas accumulation potential of the ordovician carbonate-evaporite paragenesis

system in central and eastern Ordos Basin. Earth Sci. Front. 30 (1), 30–44. https://doi.org/10.13745/j.esf.sf.2022.8.25.
Barbe, A., Grimalt, J.O., Pueyo, J.J., et al., 1990. Characterization of model evaporitic environments through the study of lipid components. Org. Geochem. 16 (4), 815–828. https://doi.org/10.1016/0146-6380(90)90120-O.
Behar, F., Vandenbroucke, M., Tang, Y., et al., 1997. Thermal cracking of kerogen in open and closed systems: determination of kinetic parameters and stoichiometric coefficients for oil and gas generation. Org. Geochem. 26 (5), 321–339. https://doi.org/10.1016/S0146-6380(97)00014-4.
Bertrand, P., Behar, F., Durand, B., 1986. Composition of potential oil from humic coals in relation to their petrographic nature. Org. Geochem. 10 (1), 601–608. https://doi.org/10.1016/0146-6380(86)90056-2.
Burnham, A.K., Braun, R.L., Gregg, H.R., et al., 1987. Comparison of methods for measuring kerogen pyrolysis rates and fitting kinetic parameters. Energy Fuel. 1 (6), 452–458. https://doi.org/10.1021/ef00006a001.
Cao, J., Zhang, R.J., Zhi, D.M., et al., 2025. Unique bimodal oil generation of alkaline-saline lacustrine source rock: evidences, modeland mechanism of organic-inorganic interactions. Sci. China Earth Sci. 68 (5), 1559–1582. https://doi.org/10.1007/s11430-024-1525-0.
Ding, K.L., Mei, P., Luo, Y., 2016. Pyrite-hydrocarbon interaction under hydrothermal conditions: an alternative origin of H2S and organic sulfur compounds in sedimentary environments. Acta Geol. Sin. 90 (6), 2133–2148. https://doi.org/10.1111/1755-6724.13027.
Dong, S.W., Zhang, Y.Q., et al., 2019. The Yanshan orogeny and late Mesozoic multi-plate convergence in East Asia-commemorating 90th years of the "Yanshan Orogeny". Sci. China Earth Sci. 49 (6), 913–938. https://doi.org/10.1007/s11430-017-9297-y.
Fakhraee, M., Crockford, P.W., Bauer, K.W., et al., 2025. The history of Earth's sulfur cycle. Nat. Rev. Earth Environ. 6, 106–125.
Fu, S.T., Fu, J.H., Yu, J., et al., 2018. Petroleum geological features and exploration prospect of Linhe Depression in Hetao Basin, China. Petrol. Explor. Dev. 45 (5), 803–817. https://doi.org/10.1016/S1876-3804(18)30084-3.
Fu, X.Y., Lu, J.G., Shi, Y.L., et al., 2024. Hydrocarbon generation mechanism of saline lake source rocks in Linhe depression, Hetao Basin. Nat. Gas Geosci. 35 (4), 704–717 (in Chinese). https://doi.org/10.11764/j.issn.1672-1926.2023.06.010.
Fu, Y., Wang, Z.D., Zhang, T., et al., 2025. A saline lacustrine depositional environment enhances organic matter enrichment in the Permian Lucaogou shales. Org. Geochem. 206, 105009. https://doi.org/10.1016/j.orggeochem.2025.105009.
Gao, Y.Q., He, X.P., Cheng, X., et al., 2024. Discussion on high hydrocarbon generation efficiency of saline lacustrine source rocks with low TOC: a case study of the second member of funing Formation, Qintong Sag, Subei Basin. Petrol. Reservoir Eval. Dev. 14 (5), 678–687. https://doi.org/10.13809/j.cnki.cn32-1825/te.2024.05.002.
Gong, D.Y., Liu, Z.Y., He, W.J., et al., 2024. Multiple enrichment mechanisms of organic matter in the Fengcheng Formation of Mahu Sag, Junggar Basin, NW China. Petrol. Explor. Dev. 51 (2), 292–306. https://doi.org/10.1016/S1876-3804(24)60024-8.
Grba, N., Šajnović, A., Stojanović, K., et al., 2014. Preservation of diagenetic products of β-carotene in sedimentary rocks from the Lopare Basin (Bosnia and Herzegovina). Chemie der Erde - Geochemistry 74 (1), 107–123. https://doi.org/10.1016/j.chemer.2013.10.002.
Gu, Y., Chang, X., Liu, X.T., et al., 2025. Geochemical insights into authigenic pyrite formation in central Yellow sea sediments: influence of sedimentary environment and microbial sulfate reduction. Mar. Petrol. Geol. 182, 107587. https://doi.org/10.1016/j.marpetgeo.2025.107587.
Haven, H.L.T., Leeuw, J.W.D., Peakman, T.M., et al., 1986. Anomalies in steroid and hopanoid maturity indices. Geochem. Cosmochim. Acta 50 (5), 853–855. https://doi.org/10.1016/0016-7037(86)90361-3.
He, Q.B., Chen, S.J., Li, S.X., et al., 2022. Organic geochemical characteristics and hydrocarbon generation mechanism of marine-continental transitional organic-rich shale: A case study from the Shanxi formation in the eastern margin of the Ordos Basin. Journal of Petroleum Science & Engineering 219, 111116. https://doi.org/10.1016/j.petrol.2022.111116.
Holba, A.G., Dzou, L.I., Wood, G.D., et al., 2003. Application of tetracyclic polyprenoids as indicators of input from fresh-brackish water environments. Org. Geochem. 34 (3), 441–469. https://doi.org/10.1016/S0146-6380(02)00193-6.
Hu, M.J., Cheng, Z.Q., Zhang, M.Y., et al., 2014. Effect of calcite, kaolinite, gypsum, and montmorillonite on Huadian oil shale kerogen pyrolysis. Energy Fuel. 28 (3), 1860–1867. https://doi.org/10.1021/ef4024417.
Jin, J., Xian, B.Z., Lian, L.X., et al., 2023. Reformation of deep clastic reservoirs with different diagenetic intensities by microfractures during late rapid deep burial: implications from diagenetic physical simulation of Cretaceous Qingshuihe Formation in the southern margin of Junggar Basin, NW China. Petrol. Explor. Dev. 50 (2), 346–359. https://doi.org/10.1016/S1876-3804(23)60392-1.
Jin, X.F., Song, J., Wei, H., et al., 1998. Twice hydrocarbon-generating mechanism of sporopollen during thermo-pressurized simulation. Petrol. Explor. Dev. 25 (4), 43752.
Kelts, K., 1988. Environments of deposition of lacustrine petroleum source rocks: an introduction. Geol. Soc. Lond. Spec. Publ. 40 (1), 3–26. https://doi.org/10.1144/GSL.SP.1988.040.01.02.
Klemme, H.D., Ulmishek, G.F., 1991. Effective petroleum source rocks of the world: stratigraphic distribution and controlling depositional factors. AAPG (Am. Assoc. Pet. Geol.) Bull. 75 (12), 1809–1851. https://doi.org/10.1306/0C9B2A47-1710-11D7-8645000102C1865D.
Lewan, M.D., 1998. Sulphur-radical control on petroleum formation rates. Nature 391 (6663), 164–166. https://doi.org/10.1038/34391.
Lewan, M.D., Ruble, T.E., 2002. Comparison of petroleum generation kinetics by isothermal hydrous and nonisothermal open-system pyrolysis. Org. Geochem. 33 (12), 1457–1475. https://doi.org/10.1016/S0146-6380(02)00182-1.
Li, C.X., Liu, Z., Wang, S.C., et al., 2022. Prediction of major source rocks distribution in the transition from depressed to rifted basin using seismic and geological data: the Guyang to Linhe Formations in the Linhe Depression, Hetao Basin, China. J. Petrol. Sci. Eng. 214, 110472. https://doi.org/10.1016/j.petrol.2022.110472.
Li, G.X., Zhang, B., Wu, K.Y., et al., 2023. Low organic matter abundance and highly efficient hydrocarbon generation of saline source rock in the Qaidam Basin, NW China. Petrol. Explor. Dev. 50 (5), 1030–1044. https://doi.org/10.1016/S1876-3804(23)60447-1.
Li, Q.Q., Xu, S., Hao, F., et al., 2021. Geochemical characteristics and organic matter accumulation of argillaceous dolomite in a saline lacustrine basin: a case study from the paleogene xingouzui formation, Jianghan Basin, China. Mar. Petrol. Geol. 128, 105041. https://doi.org/10.1016/j.marpetgeo.2021.105041.
Liang, C., Yang, B., Cao, Y.C., et al., 2024. Salinization mechanism of lakes and controls on organic matter enrichment: from present to deep-time records. Earth Sci. Rev. 251, 104720. https://doi.org/10.1016/j.earscirev.2024.104720.
Liang, H.R., Xu, F.H., Grice, K., et al., 2020b. Kinetics of oil generation from brackish-lacustrine source rocks in the southern Bohai sea, East China. Org. Geochem. 139, 103945. https://doi.org/10.1016/j.orggeochem.2019.103945.
Liang, H., Xu, G.S., Xu, F.H., et al., 2020a. Oil generation of lacustrine type II shale: a case study of the Shahejie Formation, Laizhou Bay Sag, Bohai Bay Basin (China). J. Petrol. Sci. Eng. 195, 107839. https://doi.org/10.1016/j.petrol.2020.107839.
Liu, Y.Z., Shi, W.Z., Hu, Q.H., et al., 2024. The mechanism of organic matter accumulation in the archipelago marine sediments: insights from the middle Devonian Givetian mudstone with low TOC in the Youjiang Basin, South China. Mar. Petrol. Geol. 160, 106626. https://doi.org/10.1016/j.marpetgeo.2023.106626.
Lu, L., Chen, S.G., Li, Z.F., et al., 2022. Sedimentary evolution and petroleum potential of the Cretaceous to Paleogene in Linhe Depression, Hetao Basin. J. Palaeogeogr. 24 (2), 308–331. https://doi.org/10.7605/gdlxb.2022.02.022 (in Chinese).
Luo, L.Y., Li, Y., Wu, Y.Y., et al., 2026. Influence of ultra-deep solid bitumen on carbonate reservoir properties and gas saturation correction. Fuel 420, 138900. https://doi.org/10.1016/j.fuel.2026.138900.
Ma, X.X., Zheng, J.J., Zheng, G.D., et al., 2016. Influence of pyrite on hydrocarbon generation during pyrolysis of type-III kerogen. Fuel 167, 329–336. https://doi.org/10.1016/j.fuel.2015.11.069.
Machel, H.G., 2001. Bacterial and thermochemical sulfate reduction in diagenetic settings — old and new insights. Sediment. Geol. 140 (1), 143–175. https://doi.org/10.1016/S0037-0738(00)00176-7.
Meng, Q.Q., Li, J.Z., Liu, W.H., et al., 2022. Simulation study on the effect of gypsum-salt content on hydrocarbon generation in mature stage shale. Special Oil Gas Reservoirs 29 (5), 113–118 (in Chinese). https://doi.org/10.3969/j.issn.1006-6535.2022.05.016.
Meshoulam, A., Ellis, S.G., Ahmad, S.W., et al., 2016. Study of thermochemical sulfate reduction mechanism using compound specific sulfur isotope analysis. Geochem. Cosmochim. Acta 188, 73–92. https://doi.org/10.1016/j.gca.2016.05.026, 2016.
Ola, P.S., Aidi, A.K., Bankole, O.M., 2018. Clay mineral diagenesis and source rock assessment in the Bornu Basin, Nigeria: implications for thermal maturity and source rock potential. Mar. Petrol. Geol. 89, 653–664. https://doi.org/10.1016/j.marpetgeo.2017.10.031.
Peters, K.E., 1986. Guidelines for evaluating petroleum source rock using programmed pyrolysis. Am. Assoc. Petrol. Geol. Bull. 70 (3), 318–329. https://doi.org/10.1306/94885688-1704-11D7-8645000102C1865D.
Peters, K.E., Moldowan, J.M., 1993. The Biomarker Guide. Prentice Hall, Englewood Cliffs, New Jersey, p. 363.
Peters, K., Walters, K., Moldowan, J., 2005. The Biomarker Guide In: Biomarkers and Isotopes in the Environment and Human History, second ed. 1. Cambridge University Press, UK.
Peters, K.E., Burnham, A.K., Welte, C.C., 2015. Petroleum generation kinetics: single versus multiple heatingramp open-system pyrolysis. AAPG Bull. 99 (4), 591–616. https://doi.org/10.1306/11141414080.
Qin, J.Z., Zheng, L.J., Tenger, 2007. Study on the restitution coefficient of original total organic carbon for high mature marine source rocks. Front. Earth Sci. 1 (4), 482–490. https://doi.org/10.1007/s11707-007-0059-5.
Rahman, M.H., Kennedy, M., Löhr, S., et al., 2018. The influence of shale depositional fabric on the kinetics of hydrocarbon generation through control of mineral surface contact area on clay catalysis. Geochem. Cosmochim. Acta 220, 429–448. https://doi.org/10.1016/j.gca.2017.10.012.
Schenk, H.J., Dieckmann, V., 2004. Prediction of petroleum formation: the influence of laboratory heating rates on kinetic parameters and geological extrapolations. Mar. Petrol. Geol. 21 (1), 79–85. https://doi.org/10.1016/j.marpetgeo.2003.11.004.
Sun, X., Zhang, T.W., Sun, Y.G., et al., 2016. Geochemical evidence of organic matter source input and depositional environments in the lower and upper Eagle Ford Formation, south Texas. Org. Geochem. 98, 66–81. https://doi.org/10.1016/j.orggeochem.2016.05.018.
SY/T 5258-1991 (Oil and Gas Industry Standards of P. R. China), 1991. Biomarker Chromatography-Mass Spectrometry Analysis and Identification Method.
SY/T 5779-1995 (Oil and Gas Industry Standards of P. R. China), 1995. Gas Chromatographic Analysis Method for Total Hydrocarbon of Crude Oil.

Tang, X.Q., Huang, G.H., Zhang, M., et al., 2009. Compositional characteristics andgeochemical significance of n-alkanes in process of crude oil cracking. Earth Sci. Front. 16 (6), 372–378.
Tang, Y., Cao, J., He, W.J., et al., 2021a. Development tendency of geological theory of total petroleum system: insights from the discovery of mahu large oil province. Xinjing Pet. Geol. 42 (1), 1–9. https://doi.org/10.7657/XJPG20210101 (in Chinese).
Tang, Y., He, W.J., Bai, Y.B., et al., 2021b. Source rock evaluation and hydrocarbon generation model of a Permian alkaline lakes—A case study of the fengcheng Formation in the Mahu Sag, Junggar Basin. Minerals 11 (6), 644. https://doi.org/10.3390/MIN11060644.
Tissot, B.P., Welte, D.G., 1984. Petroleum Formation and Occurrence, second ed. Springer-Verlag, Berlin, p. 699.
Tribovillard, N., Algeo, T.J., Baudin, F., et al., 2009. Environmental analysis of paleoceanographic systems based onmolybdenum-uranium covariation. Chem. Geol. 268 (3), 211–225. https://doi.org/10.1016/j.chemgeo.2011.09.009.
Vivian, A.D.F., Júlio, C.D.S., Bruna, R.R., et al., 2022. Source rock potential, main depocenters, and CO_2 occurrence in the pre-salt section of Santos Basin, southeast Brazil. J. South Am. Earth Sci. 115, 103760. https://doi.org/10.1016/j.jsames.2022.103760.
Wang, Q.T., Hong, L., Greenwood, P., Shen, C.C., Liu, J.Z., Peng, P.A., 2013. Gas evolution during kerogen pyrolysis of Estonian Kukersite shale in confined gold tube system. Org. Geochem. 65 (1), 74–82. https://doi.org/10.1016/j.orggeochem.2013.10.006.
Wang, Y., Wu, J., Jin, X., et al., 2023. Sulfur-bearing free radicals promote the hydrocarbon generation of sedimentary organic matter via a hydrogen transfer mechanism. Geochimica 52 (2), 172–179. https://doi.org/10.19700/j.0379-1726.2023.02.004.
Wang, Z.X., Tang, Y.J., Wang, Y.L., et al., 2020. Kinetics of shale oil generation from kerogen in saline basin and its exploration significance: an example from the Eocene Qianjiang Formation, Jianghan Basin, China. J. Anal. Appl. Pyrolysis 150. https://doi.org/10.1016/j.jaap.2020.104885.
Warren, J.K., 2006. Evaporites: Sediments, Resources and Hydrocarbons. Springer, Berlin,Heidelberg.
Warren, J.K., 2011. Evaporitic Source Rocks: Mesohaline Responses to Cycles of "Famine or Feast" in Layered Brines, 43. International Association of Sedimentologists Special Publication, pp. 315–392.
Wu, S.C., Chen, L., Xiong, M., et al., 2024. Depositional conditions of shale lithofacies during the late ordovician–early Silurian in the Upper Yangtze area, SW China: responses to sea-level changes. Mar. Petrol. Geol. 161, 106696. https://doi.org/10.1016/j.marpetgeo.2024.106696.
Xia, L.W., Cao, J., Wang, T.T., et al., 2024. Deep-time alkaline lake enigma: rare or undiscovered? Earth Sci. Rev. 253, 104785. https://doi.org/10.1016/j.earscirev.
Xia, X.Y., Ellis, S.G., Ma, Q.S., et al., 2014. Compositional and stable carbon isotopic fractionation during non-autocatalytic thermochemical sulfate reduction by gaseous hydrocarbons. Geochem. Cosmochim. Acta 139, 472–486. https://doi.org/10.1016/j.gca.2014.05.004.
Xiang, B.L., Li, E.T., Gao, X.W., et al., 2016. Petroleum generation kinetics for Permian lacustrine source rocks in the Junggar Basin, NW China. Org. Geochem. 98, 1–17. https://doi.org/10.1016/j.orggeochem.2016.05.003.
Xiao, Z.L., Chen, S.J., Li, Y., et al., 2021. Local high-salinity source rock and origin of crude oil in the xianshuiquan structure in the northwestern Qaidam Basin, China. J. Petrol. Sci. Eng. 198, 108233. https://doi.org/10.1016/j.petrol.2020.108233.
Zhang, D.W., 2019. Accumulation conditions and key technologies for exploration and development in sebei gas field in Qaidam Basin, NW China. Petrol. Res. 4 (3), 191–211. https://doi.org/10.1016/j.ptlrs.2019.05.003.
Zhang, R.F., He, H.Q., Zhu, Q.Z., et al., 2023. Petroleum geological features and hydrocarbon enrichment of Linhe depression in Hetao Basin, NW China. Petrol. Explor. Dev. 50 (4), 798–811. https://doi.org/10.1016/S1876-3804(23)60429-X.
Zhang, R.F., Lu, J.G., Shi, Y.L., et al., 2025. Sedimentary environment and controlling factors of carotane development: a case study of Linhe depression in Hetao Basin. Petrol. Sci. Technol. 43 (1), 25–39. https://doi.org/10.1080/10916466.2023.2276234.
Zhang, T., Ellis, S.G., Walters, C.C., et al., 2007. Geochemical signatures of thermochemical sulfate reduction in controlled hydrous pyrolysis experiments. Org. Geochem. 39 (3), 308–328. https://doi.org/10.1016/j.orggeochem.2007.12.007, 2007.
Zhang, Y.Y., Li, Y., Zhang, X.Y., et al., 2026. Influence of solid bitumen on reservoir physical properties and logging parameters and its quantitative evaluation method. Chin. J. Geophys. 69 (2), 883–901. https://doi.org/10.6038/cjg2025S0732.
Zhao, W.Z., Zhang, B., Wang, X.M., et al., 2021. Differences in source kitchens for lacustrine in-source and out-of-source hydrocarbon accumulations. Petrol. Explor. Dev. 48 (3), 541–554. https://doi.org/10.1016/S1876-3804(21)60044-7.
Zhi, D.M., Tang, Y., He, W.J., et al., 2021. Orderly coexistence and accumulation models of conventional and unconventional hydrocarbons in Lower Permian Fengcheng Formation, Mahu sag, Junggar Basin. Petrol. Explor. Dev. 48 (1), 43–59. https://doi.org/10.1016/S1876-3804(21)60004-6.
Zhong, N.N., Lu, S.F., Huang, Z.L., et al., 2004. The change in total organic carbon (TOC) and its governing factors during the hydrocarbon generation evolution of source rocks. Sci. China, Ser. D Earth Sci. 34 (201), 120–126.
Yang, R.B., Luo, Q.Y., Wu, J.P., et al., 2025. Hydrocarbon generation potential and organic carbon enrichment in evaporitic lacustrine source rocks from the Qianjiang Formation, Jianghan Basin (Central China): an integrated geochemical-petrological investigation. Int. J. Coal Geol. 307, 104827. https://doi.org/10.1016/j.coal.2025.104827.
Yu, J.W., Fu, H., Zhang, Z, et al., 2018. Petrophysical facies of Toutunhe Formation in Fudong slope area, Junggar Basin. Oil and Gas Geology 39 (1), 129–139. https://doi.org/10.11743/ogg20180113.